Electrophoresis as a simple method to detect deleterious actions of engineered nanoparticles on living cells

Elise Vouriot, Isabelle Bihannic, Audrey Beaussart, Yves Waldvogel, Angelina Razafitianamaharavo, Tânia Ribeiro, José Paulo S. Farinha, Christophe Beloin, Jérôme F.L Duval

Electrophoresis as a simple method to detect deleterious actions of engineered nanoparticles on living cells

Elise Vouriot,[a] Isabelle Bihannic,[a,⊥] Audrey Beaussart, [a,⊥] Yves Waldvogel,[a]
Angelina Razafitianamaharavo,[a] Tania Ribeiro,[b] José Paulo S. Farinha,[b] Christophe Beloin,[c]
Jérôme F.L. Duval[a,*]

[a] Université de Lorraine, CNRS, LIEC (Laboratoire Interdisciplinaire des Environnements Continentaux), UMR 7360, Vandoeuvre-lès-Nancy F-54501, France.
[b] Centro de Química-Física Molecular and IN - Institute of Nanoscience and Nanotechnology, Instituto Superior Técnico, University of Lisbon, 1049-001, Lisboa, Portugal.
[c] Institut Pasteur, Unité Génétique des Biofilms, F-75724 Paris 15, France.

[⊥] These authors equally contributed to this work.
[*] Corresponding author: jerome.duval@univ-lorraine.fr

Abstract:

The release of engineered nanoparticles (NPs) in the environment may have profound implications for the health of aquatic biota. In this study, we evidence that the initial stage of NPs action on bacteria can be detected upon measurement of the electrophoretic fingerprints of mixed NPs-cells dispersions. Such electrokinetic signatures reflect a modification of the physicochemical cells and NPs surface properties following changes in cell envelope organization, subsequent intracellular material release and/or biomolecules cell excretion. The demonstration is based on a thorough investigation of the electrohydrodynamic features of genetically engineered *Escherichia coli* bacteria exhibiting distinct surface phenotypes (presence of adhesive YeeJ large proteins or F-pili proteinaceous filaments) exposed to silica NPs (65 nm radius) functionalized by $-NH_2$ terminal groups. At pH 7, electrostatics prevents interactions between bacteria and $SiNH_2$ NPs, regardless of the NPs concentration considered ($0\text{-}10^{-2}$ g L^{-1} range). At pH 3, electrostatically-driven interactions allow intimate contacts between NPs and bacteria. In turn, significant modulation of the electrophoretic determinants of cells and NPs are generated due to cells envelope alteration and bio-corona acquisition by NPs. Differentiated roles of the cell surface appendages in the mediation of NPs impacts are evidenced by the measured dependence of electropherograms on cell surface phenotype and NPs concentration. Cell morphology and surface roughness, evaluated by Atomic Force Microscopy (AFM) in liquid, confirm the pH and NPs concentration conditions where NPs-cells interactions are operational. Combination of electrokinetics and AFM further pinpoints heterogeneities in cells response at the single cell and population scales. Altogether, results show that electrokinetics is suitable to detect the preliminary stage of events leading to NPs toxicity toward microorganisms.

Environmental context:

Attractive interactions and subsequent contacts between NPs and microorganisms are the first steps of a chain of events leading to adverse NPs effects toward cells. Herein we show that the electrophoretic response of complex mixtures of engineered NPs (silica NPs) and bacteria (*E. coli*)

reflects initial NPs-mediated cell surface damages. We thus provide a promising option for a rapid electrokinetics-based detection of deleterious actions of NPs on biological cells.

1. Introduction

Over the past decades, nanomaterials and related products have gained a prominent importance in our everyday life. In particular, engineered nanoparticles (NPs) are now commonly used in various industries such as food-processing, electronics or cosmetics as well as in numerous pharmaceutical and biomedical applications (Ju-Nam and Lead 2008; Svenson 2009). NPs are released in the environment and their dissemination may severely impact on the proper functioning of ecosystems. For the sake of illustration, NPs are known to affect the speciation of essential trace metal elements (Duval 2017), to disturb their biogeochemical cycling (Chai et al. 2015), to modify microbial diversity (Yang et al. 2013), or to affect cells growth (El Badawy et al. 2011), cells viability (Choi et al. 2010; Stoimenov et al. 2002) and cells ability to form biofilms (Ikuma et al. 2015; Neal 2008; Peulen and Wilkinson 2011). These issues have motivated the scientific community to deploy important efforts for investigating the mechanisms governing the interactions between NPs and bacteria at various spatial scales (Beddoes et al. 2015; Choi et al. 2010; Shang et al. 2014), and for identifying implications in terms of adverse outcome pathways and toxicity (Colvin 2004; Kleinstreuer et al. 2016; Moore 2006; Velzeboer et al. 2008). Acquiring such basic knowledge is a mandatory condition for the elaboration of environmental remediation strategies or the development of new industrial practice, *e.g.* the eco-friendly design of novel nanoparticulate products (Ingale and Chaudhari 2013).

The magnitude and nature of the interactions operational between bacterial cells and NPs (steric, electrostatic, van der Waals, hydrophobic and/or lock-and-key) are intimately connected to the physicochemical composition and spatial organization of the cell envelope (Beaussart et al. 2018a; Jacobson et al. 2015; Jiang et al. 2010; Monopoli et al. 2012). The latter include differences in cell wall structures (*e.g.* Gram+ *vs.* Gram- bacteria) (Beveridge and Graham 1991) or the presence of peripheral appendages, *e.g.* fimbriae, pili, lipopolysaccharides or flagella that mediate cell resistance and binding to NPs (Beaussart et al. 2018a; Jacobson et al. 2015; Jiang et al. 2010; Mathelié-Guinlet et al. 2018). Together with the defining physicochemical properties of NPs (*i.e.* NP size, charge, or hydrophobic/hydrophilic balance), the physicochemical functionalities of cell envelopes determine whether or not contact between cells and NPs takes place (Beaussart et al. 2018a; Beddoes et al. 2015; Phillips et al. 2008; Thill et al. 2006). As such, the existence of NPs-cells attractive interactions is the required condition for NPs to induce possible cell surface alterations, cell dysfunction and toxicity effects (Choi et al. 2010; Hayden et al. 2012; Planchon et al. 2013). This situation obviously excludes NPs whose action mode does not require any contact with- or binding to the biological target, *e.g.* metallic NPs whose dissolution in aqueous media releases metal ions at the origin of adverse effects on biota (Choi et al. 2010).

Various techniques may be employed for measuring the interactions between biological cells and NPs, and/or evaluating their respective electrostatic surface properties. Among them, protolytic titrations allow the determination of surface charges of biotic and abiotic colloids (Van Der Wal et al. 1997). Though robust for abiotic systems like NPs, in case of *e.g.* bacteria the method suffers from the difficulty to discriminate between protons acting as charge determining-ions and protons that are released or uptaken by cells for metabolic purpose. As an alternative, Atomic Force Microscopy (AFM) now makes it possible to address the repartition of cell surface charges at the single cell level, or even measure the governing interactions between a given bacterium and a single NP with diameter less than 10 nm (Beaussart et al. 2018a). However, the inherent and obvious limit of such spatially-resolved AFM-based studies is the possible analysis of a restricted number of cells only. Besides, in some cases, the AFM probe jumps in contact with the investigated biosurface at

sufficiently low separation distances, which may render difficult any quantitative detection of short range electrostatic attraction events. Electrophoresis probably belongs to the most commonly adopted methods for addressing the electrostatic properties of cells surface or NPs. It consists in the application of a direct current electric field between two electrodes positioned in a solution containing the (bio)colloids of interest. Field-induced migration of the latter is tracked by dedicated optical or light-scattering systems depending on (bio)particle size. The so-evaluated (bio)particle electrophoretic mobility is then commonly converted into a zeta potential value and a surface charge density using classical electrokinetic and double layer theories (Planchon et al. 2013; Rowenczyk et al. 2017; Silva et al. 2014). Application of the latter is however strictly valid for hard particles (*i.e.* particles impermeable to ions and fluid flow) at the surface of which a slip plane can be unambiguously identified (Delgado et al. 2005), and the concept of zeta potential is physically meaningless for soft (*i.e.* ion- and flow-permeable) particles like bacteria or NPs decorated by polymeric coatings (Beaussart et al. 2018a; Dague et al. 2006; Duval and Gaboriaud 2010; Duval and Ohshima 2006; Li et al. 2010; López-Viota et al. 2009; Ohshima 1995). The electrophoretic mobility of soft NPs and bacteria is a measurable quantity that depends not only on the density of charges they carry, but also on the spatial distributions of the charges in the directions parallel and perpendicular to the interface they form with the outer solution (Duval and Gaboriaud 2010; Hill et al. 2003; Moussa et al. 2015), on their dimension (Duval and Ohshima 2006; Hill et al. 2003; Ohshima 1995), on their concentration in solution pending overlap of double layers and/or of hydrodynamic spheres of action between neighboring particles (Maurya et al. 2018), on their zwitterionic character if applicable (Beaussart et al. 2018b, Moussa et al. 2015), on the length and density of their (bio)polymeric fringe (Duval and Gaboriaud 2010; Francius et al. 2011), and on the physicochemical composition of the dispersing medium (pH, ionic strength, nature of the electrolyte) (Duval and Gaboriaud 2010; López-León et al. 2005; Ohshima 1995; Pagnout et al. 2012). Electrophoresis and analysis of so-called electropherograms may further serve to detect -within *e.g.* a given bacteria dispersion- the presence of subpopulations of cells defined by distinct electrostatic surface properties (Dague et al. 2006).

To the best of our knowledge, there has been no method reported so far for achieving a rapid *in situ* detection of attractive interactions between NPs and bacteria, and for analyzing heterogeneity in cells response to NPs. Such a method would however add value to preliminary and rapid-screening risk assessment procedures. The elements above indicate that electrophoresis could be used for that purpose. Indeed, NPs generally lead to a modification of cell surface features either as a result of NPs ad-/ab-sorptions (Thill et al. 2006; Zeyons et al. 2009), NPs-mediated cell abrasion and cell wall integrity loss (Brayner et al. 2006; Hayden et al. 2012; Huang et al. 2008; Mathelié-Guinlet et al. 2017; Mecke et al. 2005; Shrivastava et al. 2007), and subsequent release of intracellular material (Hayden et al. 2012; Mathelié-guinlet 2017) that potentially decorates or aggregates NPs in solution. In turn, the electrophoretic cells surface properties and possibly those of the NPs are expected to differ from their pristine values. The purpose of the current study is to explore the potentialities of electrophoresis to discriminate between cells affected or not by NPs action. This requires the analysis of the electrophoretic behavior of NPs-cells mixtures, which is so far missing from nanotoxicology literature that mainly reports zeta potential-based assignment of (bio)particulate monospecies. To reach the aforementioned objective, the electrokinetic fingerprints of mixed suspensions of model NPs (silica NPs decorated by $-NH_2$ groups, 130 nm in diameter (Ribeiro et al. 2017, 2014)) and *Escherichia coli* (*E. coli*) cells harboring surface appendages (F-pili (Beloin et al. 2010) or YeeJ surface proteins (Martinez-Gil et al. 2017)) are analyzed as a function of NPs concentration and solution pH. Results are further complemented by AFM images of bacterial cells in liquid medium in order to visualize cell surface state and NP-mediated cell damage. Overall, the conclusions comfort the

potentialities of electrophoresis for assessing the first stage of NPs action toward the surface of biological cells.

2. Material and Methods

2.1 Bacteria

The *Escherichia coli* K12 mutant strains adopted in this work are listed in **Table 1** where relevant information on their expressed surface appendages, genotype and antibiotic resistance can be found. The genetically modified strains were kindly provided by the Institut Pasteur of Paris (Department of Microbiology, Unité de Génétique des Biofilms). The here-used isogenic strains were generated from *E. coli* MG1655 by construction of linear DNA fragments using Polymerase Chain Reaction (PCR) and the constructions were inserted in *E. coli* genome by λ red recombination (Chaveroche et al. 2000). Two cell surface phenotypes were considered: cell membranes exclusively decorated by either F-pili (E2302) appendages (Beloin et al. 2010) or by YeeJ large surface proteins (E2551) (Martinez-Gil et al. 2017). Nude bacteria (E2152), devoid of any of these two surface appendages, served as a control strain. The cells strains E2302, E2551 and E2152 adopted here did not further harbor Ag43 adhesins nor type 1 fimbriae at their surface, as further specified in **Table 1**. F-pili are long flexible proteinaceous filaments with diameter below 10 nm (Costa et al. 2016; Wang et al. 2009) and their length may range from 10 µm to 100 µm under fully stretched configuration. The number of F-pili typically found on bacterial cells is between 1 and 3 (Dubey and Maheshwari 1999; Reisner et al. 2003; Wang et al. 2009). These cell surface components play a key role in biofilm formation as they promote initial cell adhesion to abiotic surfaces (Beloin et al. 2010; Flemming et al. 2016). In addition, the F-pili is well known as mediator of conjugative transfer of plasmids (Silverman 1997). As far as YeeJ proteins are concerned, they also promote biofilm adhesion on abiotic surfaces, their theoretical isoelectric point is 4.79 and their theoretical molecular weight is 244 kDa (Martinez-Gil et al. 2017).

Using the relevant antibiotics listed in **Table 1**, bacteria were pre-grown in Lysogeny Broth (LB) medium (BD Difco®) for 10 h at 37°C under 160 rpm agitation and aerobic conditions. The pre-culture was then diluted to a 1:50 ratio in minimum M63B1 medium containing 0.4% w/w glucose and appropriate antibiotics (hereafter called M63B1glu medium). In details, this M63B1glu medium contained 13.6 g L^{-1} KH_2PO_4 (Sigma-Aldrich®), 2 g L^{-1} $(NH_4)_2SO_4$ (Emsure®), 0.1 g L^{-1} $MgSO_4,7H_2O$ (Emsure®), 5.10^{-4} g L^{-1} $FeSO_4,7H_2O$ (Sigma-Aldrich®), 1.10^{-3} g L^{-1} thiamine (Roth®) and 4 g L^{-1} glucose (Sigma®). The pre-culture was further grown for 12 h at 37°C, 160 rpm agitation under aerobic conditions. Then, cells culture was re-suspended in fresh M61B1glu, without antibiotics, at an OD_{600} of 0.05, and finally cultured at 37°C, 160 rpm until an OD_{600} value of 0.5 was reached.

<u>*Preparation of cells suspensions for electrophoresis measurements on bacteria in the absence of NPs (results given in **Figure 3**).*</u> Bacteria cultured as detailed above were first centrifuged for 5 min at 5000×g and then re-suspended in 10 mM KNO_3 (Sigma-Aldrich®, purity > 99%) so as to reach an OD_{600} of 0.2. Then, batches of cells suspended in 1 mM to 250 mM KNO_3 final electrolyte concentration were prepared in such a way that a final OD_{600} of 0.02 was reached. For that purpose, appropriate volumes of 2M KNO_3 electrolyte, of ultrapure water (milli-Q® water) and of the aforementioned cells suspensions (OD_{600}=0.2, 10 mM KNO_3) were added to get a total final suspension volume of 80 ml. The pH of the resulting cell suspension was then adjusted to the desired value upon addition of HNO_3 and KOH (10^{-2}-10^{-1} M, Fluka®) under agitation conditions (500-700 rpm) and the added acid/base volume did not correspond to more than 1% of the total suspension volume.

Preparation of mixed NPs-cells suspensions for electrophoretic mobility measurements on bacteria in the presence of NPs (***Figure 4***). For the electrokinetic experiments conducted on suspensions containing both bacterial cells and NPs (binary systems), bacteria were first centrifuged for 5 min at 5000×g and then re-suspended in 1 mM KNO_3 (Sigma-Aldrich®, purity > 99%) so as to reach an OD_{600} of 0.4. Appropriate volumes of (i) separately prepared 1 mM KNO_3 NPs suspension at 10^{-1} g L^{-1} (pH 3 or 7) obtained after 20 min sonication, of (ii) bacteria suspension (OD_{600}=0.4, 1 mM KNO_3) and of (iii) 1 mM KNO_3 solution (pH 3 or 7) were then mixed under agitation conditions (500-700 rpm) so as to achieve a final solution composition (28 ml total volume) with NPs concentration in the range 0 g L^{-1}-10^{-2} g L^{-1}, and an OD_{600} of 0.02. The suspension pH was controlled and readjusted if necessary to pH 3 or 7. Again, the added acid/base volume did not correspond to more than 1% of the total suspension volume. Mobility measurements in such NPs-cells mixtures were conducted 15 minutes after introduction of the NPs. This time delay thus defines here the duration of the cells exposition to $SiNH_2$ NPs. Experiments were carried out twice on freshly prepared samples. Under the conditions applicable in **Figure 4**, the OD_{600nm} is 0.02 and the maximum NPs concentration tested is 10^{-2} g/L, which makes a ratio 'mass of NPs per cell' of about 0.5 pg/cell. This order of magnitude is well in agreement with that considered in other studies (Mathelié-Guinlet et al. 2018).

2.2 Silica nanoparticles (SiNPs in short)

SiNPs were kindly provided by Instituto Superior Técnico, University of Lisboa, Portugal. They were synthetized according to modified Stöber protocol as described elsewhere (Crucho et al. 2017; Ribeiro et al. 2017, 2014; Stöber et al. 1968). Briefly, silica NPs were generated upon hydrolysis and condensation of tetraethoxysilane (TEOS) in ethanol in the presence of ammonia as catalyst. The modification of the SiNPs surface was performed in dry toluene under argon atmosphere (Crucho et al. 2017; Ribeiro et al. 2014), which results in SiNPs decorated by 2 NH_2 surface groups per nm^2, as determined by nuclear magnetic resonance (Crucho et al. 2017). The diameter of the synthesized particles is 130 nm ± 10 nm, as inferred from Transmission Electronic Microscopy (TEM) measurements (Supplementary Material, **Figure S1**). Dried $SiNH_2$ NPs were dispersed in 0.1 mM or 1 mM KNO_3 electrolyte to obtain a final 0.1 g L^{-1} NPs concentration. For that purpose, the appropriate weight of NPs was added to half of the desired volume of KNO_3 solution under 1000 rpm agitation conditions for 1 min, and the volume was filled with 0.1 mM or 1 mM KNO_3 to reach the final targeted volume. The so-obtained NPs suspension (pH 7) was finally stirred for 24 h at 1000 rpm. Prior to use of NPs suspensions, the latter were systematically sonicated for 20 min and then left at rest for 1 h.

2.3 Size and electrophoretic mobility measurements

Electrophoretic mobilities (μ) of NPs and bacteria considered separately were measured using Zetasizer NanoZS (Malvern Instruments®, UK) and Zetaphoremeter IV (CAD Instrumentations®, Les Essarts le Roi, France), respectively. The former apparatus is well suited for particles with diameter in the range 1 nm to 6 µm (size measurements) and 5 nm to 10 µm (electrophoretic mobility measurements), and the latter for larger systems with size in the range 0.1 µm to 50 µm (mobility measurements). For mobility measurements performed in the NPs-cells binary systems, the Zetaphoremeter equipment was adopted because our primary interest is the detection of changes in the electrophoretic signature of cells following their interaction with NPs.

2.3.1 NPs electrophoretic mobility and size measurements

Size measurements

The hydrodynamic diameter of $SiNH_2$ NPs was measured at solution pH 3 and 7 as a function of KNO_3 salt concentration (0.1-250 mM) using Dynamic Light Scattering (DLS) (Zetasizer NanoZS, Malvern®)

with a 633 nm laser. The particle diffusion coefficient was obtained from the correlation of the measured scattered intensity and converted to hydrodynamic diameter using Stokes-Einstein equation. Results are reported here in the form of particle number-size distributions. The NPs suspensions used for size measurements were prepared from the NPs suspensions obtained in §2.2 after proper dilution or addition of KNO_3 salt and pH adjustment using HNO_3 (10^{-1}-10^{-2}M Fluka®) or KOH (10^{-1}-10^{-2}M, Fluka®).

Electrophoretic mobility measurements

The electrophoretic mobility of $SiNH_2$ NPs was measured as a function of pH (3 to 9) and KNO_3 salt concentration in the range 0.1 mM to 250 mM at 25°C using Zetasizer NanoZS. A constant direct current electric field (25 V cm^{-1}) applied between two electrodes immersed in the NPs-containing solution imposes a displacement of the particles. Electrophoretic mobility was then determined using Phase Analysis Light Scattering (PALS) technology (Malvern Instruments). NPs suspensions were prepared in a way similar to that adopted for size measurements. Experiments were carried out 3 to 5 times on freshly prepared samples.

2.3.2 Cells electrophoretic mobility measurements and electrokinetics of mixed NPs-bacteria suspensions

The Zetaphoremeter was used for electrophoretic mobility measurements of bacteria and of binary NPs-bacteria systems. The instrument consists of a quartz suprasil cell, a laser and a charge-coupled device camera connected to a computer. The camera tracks the positions of the bacteria *via* a laser, and a software processes the obtained images in real time. From the displacement of the tracked cells, subjected to a constant direct-current electric field (800 V m^{-1}), the electrophoretic velocity and electrophoretic mobility were evaluated (Francius et al. 2011; Pagnout et al. 2012). The electrophoretic mobility of bacteria was measured at pH 3 and 7 as a function of KNO_3 electrolyte concentration (1-250 mM). Cells suspensions and mixed NPs-cell suspensions were prepared along the lines detailed in §2.1.

2.4 Atomic Force Microscopy (AFM) measurements

AFM imaging of bacterial cells was performed under liquid conditions using a Bruker FastScan Dimension Icon with Nanoscope V controller operated in Peak Force tapping mode at 1.0 Hz scan rate (Bruker® corporation, Palaiseau, France). This mode consists in monitoring the intermittent contact between tip and sample surface with application of a 7 nN force, at most (except 12 nN for imaging of E2302 cells at pH 3), which limits possible samples damage by the tip (NPG tips, nominal spring constant of 0.12 N m^{-1}, Bruker, AXS®, Palaiseau, France). Prior to experiments, glass slides were coated with a polycationic polymer (polyethylenimine, PEI in short) to promote electrostatic immobilization of bacterial cells. In detail, the glass slides were cleaned with 1 g L^{-1} RBS 25 solution (Sigma-Aldrich®) at 60°C for 30 min, then rinsed with milli-Q® water, subsequently immersed in a 1 g L^{-1} PEI solution (Sigma-Aldrich®, 7.5 10^6 Mw, 50 wt. % in H_2O) for 30 min and finally rinsed with milli-Q® water. 1.4 mL of bacterial suspension (of pH 3 or 7, and OD_{600} = 0.4) was deposited onto the PEI-coated slides. After 30 min, the sample was extensively rinsed with 1 mM KNO_3 solution (pH 3 or 7) and the slide was then fixed to a magnetic puck and placed into the AFM fluid-cell containing 2 mL of 1 mM KNO_3 solution at the sample pH (3 or 7). For AFM imaging of binary systems, bacteria suspensions (OD_{600} = 0.4) were first mixed with 1 mM KNO_3 NPs solution of final concentration 10^{-3} g L^{-1} under 15 min agitation conditions, similar to those adopted for preparing the mixed cells-NPs suspensions analysed by electrokinetics (§2.1). The suspensions were then deposited onto the PEI-coated slides for 30 min and rinsed with 1 mM KNO_3 solution, pH 3 or 7. For each tested condition (pH 3 or 7, presence/absence of $SiNH_2$ NPs), AFM images (256×256 pixels, 3.5 μm×3.5 μm, pixel

size=13.7 nm) were recorded on *ca.* 3 to 7 cells per strain originating from different cell cultures. Cell surface roughness features (mean value and standard deviation) were evaluated from analysis of areas (400 nm×400 nm) of 3 to 7 distinct cells imaged as detailed above.

3. Results and Discussions

Before analyzing the modulations of the electrokinetic properties of bacterial cells as a result of their interactions with $SiNH_2$ NPs, we discuss below the electrophoretic mobility properties of $SiNH_2$ NPs and of the adopted *E. coli* strains, taken separately.

3.1 Electrokinetics of $SiNH_2$ NPs and of bacteria

The dependence of the electrophoretic mobility μ of $SiNH_2$ NPs on KNO_3 electrolyte concentration and pH is reported in **Figure 1**.

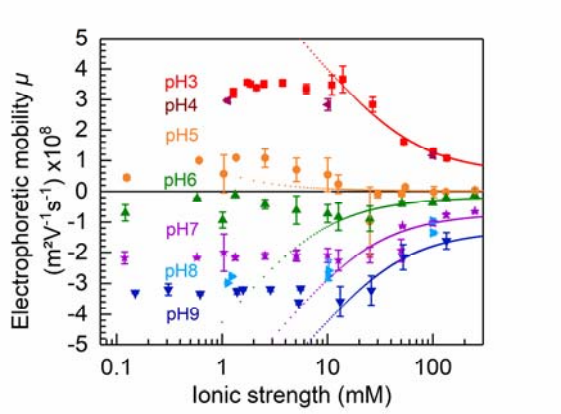

Figure 1: Electrophoretic mobility of $SiNH_2$ NPs as a function of pH (indicated) and solution ionic strength (changed upon modification of KNO_3 electrolyte concentration in solution). Colored symbols: experimental data. Lines: data reconstruction by means of Ohshima's theory (**eqs 1-4**). Measurements, performed with Zetasizer NanoZS equipment (Malvern Instruments®, UK), were carried out on 2 to 5 freshly prepared $SiNH_2$ NPs suspensions, and each of these measurements was done in triplicate. Accordingly, each point in Figure 1 is the average of 6 to 15 measurements.

The mobility μ of $SiNH_2$ NPs is negative over the whole range of tested KNO_3 concentrations at pH>6 and it is positive for pH values lower than 5-6. The underlying reversal of $SiNH_2$ NPs surface charge is surprising in view of the expected presence of amine surface groups that would lead -if solely considered- to positive NPs mobility regardless of pH and salinity conditions. The reason for this charge reversal stems from the NPs surface functionalization efficiency (2 NH_2 surface groups per nm^2), leaving a considerable amount of hydroxyl groups from the silica structure exposed to the outer aqueous solution (Crucho et al. 2017). As a result, the positive charge of the NPs stems from the protonation of $-NH_2$ groups that becomes significant with decreasing pH below *ca.* 6 (**Figure 1**), which is in agreement with typical p*K* values reported for amine groups (Diallo et al. 2004; Tajarobi et al. 2001). For pH values larger than 6, the negative charge of NPs originates from the dissociation of the surface hydroxyl groups whose contribution overwhelms that of the poorly protonated $-NH_2$ groups under such pH conditions. The comparison between $|\mu|$ reached at pH 9 and pH 3 in *e.g.* 10 mM KNO_3 suggests that the NPs surface concentration of $-NH_2$ and -OH groups is similar. With decreasing salt concentration from 100 mM to 10 mM at fixed pH, $|\mu|$ increases due to reduction of NPs surface charge screening by ions from the background electrolyte. Further decrease in electrolyte concentration results in a mobility that becomes -within experimental error- basically

independent of salt content in solution. Two reasons may be invoked for qualitatively explaining the behavior of μ at such low KNO_3 concentrations (here, below 10 mM): (i) double layer polarization effects, that tend to reduce the dependence of μ on salt concentration, as demonstrated elsewhere for highly charged polymer NPs (Duval et al. 2013), and/or (ii) changes in the spatial organization of the cationic and anionic surface charges within the thin polyelectrolytic like-layer surrounding the NPs. These latter changes also lead to moderate variations of μ on electrolyte concentration for the reasons detailed by (Moussa et al. 2015) in their electrophoresis analysis of zwitterionic carboxylate-terminated poly(amidoamine) dendrimers. In the following developments, we restrict our quantitative analysis of the electrophoretic properties of $SiNH_2$ NPs to KNO_3 concentrations larger than 10 mM with adopting the analytical model developed by Ohshima for soft particle electrokinetics (Ohshima 1995). Soft particles correspond to porous or core/shell particles whose peripheral polyelectrolyte structure is permeable to ions and fluid flow and for which the concept of zeta potential is meaningless (Duval and Gaboriaud 2010). Unlike standard zeta potential-based models strictly applicable to hard particles that are impermeable to ions and flow, soft particle representation was shown to correctly apply to silica NPs (Škvarla 2007) or to latex particles with polymeric surface layer as thin as 1 nm (Duval et al. 2013). According to Ohshima (Ohshima 1995), the mobility μ of a soft particle reads as

$$\mu = \frac{\rho_0}{\eta\lambda_0^2} + \frac{\varepsilon}{\eta}\frac{\psi^{\circ}/\kappa_m + \psi^D/\lambda_o}{1/\kappa_m + 1/\lambda_o} \quad \textbf{(1)}$$

, where ρ_0 corresponds to the effective charge density of the soft surface layer and $1/\lambda_0$ to the so-called hydrodynamic penetration length, *i.e.* the extent by which the electroosmotic flow developed under electrokinetic conditions penetrates the soft surface layer. η and ε are the dynamic viscosity and dielectric permittivity of the medium, respectively, κ_m the reciprocal Debye layer thickness in the soft surface layer, ψ^0 the surface potential located at the edge of the soft layer, and ψ^D the Donnan potential. Equation 1 holds under conditions where the particle hard core radius a and the soft surface layer thickness d well exceed the thickness of the double layer at the fluid side of the particle/solution interface, and the hydrodynamic penetration length $1/\lambda_0$ is significantly lower than d, *i.e.* $\kappa a >> 1,\ \kappa d >> 1,\ \lambda_o d >> 1$. These conditions are satisfied at sufficiently large electrolyte concentrations where polarization of electric double layers is insignificant and interfacial potentials are in line with applicability of the Debye Hückel approximation (Duval and Gaboriaud 2010; Duval and Ohshima 2006; Ohshima 1995). The quantities ψ^D, ψ^0 and κ_m all depend on charge density ρ_0 and electrolyte concentration c^{∞} (1:1 symmetrical electrolyte is considered here) according to (Ohshima 1995)

$$\psi^D = \frac{RT}{F}\sinh^{-1}\left(\frac{\rho_0}{2Fc^{\infty}}\right) \quad \textbf{(2)}$$

$$\psi^0 = \psi^D - \frac{RT}{F}\tanh\left(\frac{F\psi^D}{2RT}\right) \quad \textbf{(3)}$$

$$\kappa_m = \kappa\left\{\cosh\left(\frac{F\psi^D}{RT}\right)\right\}^{1/2} \quad \textbf{(4)}$$

, where R is the gas constant, T the absolute temperature, F the Faraday number and κ the salinity-dependent reciprocal Debye layer thickness. **Equations 1-4** successfully fitted the experimental data above 10 mM KNO_3 concentration in **Figure 1** upon adjustment of ρ_0 and $1/\lambda_0$ *via* Levenberg-Marquardt procedure. Results are given in **Table 2** for the various tested pH conditions with ρ_0 expressed in molar concentration of equivalent monovalent charges. In agreement with conclusions from previous work (Škvarla 2007), $SiNH_2$ NPs may be represented by Ohshima's soft (core/shell)

particle representation as $1/\lambda_o$ significantly deviates from 0 value (the latter strictly pertains to the limit of hard impermeable particles), in line with the presence of a thin, fuzzy polyelectrolyte layer hosting the -OH and -NH_2 surface groups. In detail, the hydrodynamic softness of $SiNH_2$ NPs stems from the non-ideality of their surface *at the molecular scale*, materialized by the presence of asperities, depressions and non-homogeneous distributions of functional groups along- and perpendicular to- their surface. In turn, it is impossible to locate a slip plane for such particulate systems and to define rigorously a common planar location for all ionogenic groups (and therewith defined a *surface charge* density), as traditionally done for the ideal case of hard particles. A way to apprehend these deviations is to reason in terms of volume charge density and to consider that the electroosmotic flow profile *gradually* (and not abruptly as for hard particles) drops to zero from the bulk solution to the particle phase with a decay length scale given by $1/\lambda_o$. These elements explain why particles like $SiNH_2$ NPs behave as soft particles. Ohshima's model overestimates the magnitude of μ for all pH conditions at KNO_3 concentrations below 10 mM where possible double layer polarization, structural modulation of the polyelectrolyte surface layer and deviation from linearized Poisson-Boltzmann and Donnan electrostatics come into play, all these features being discarded in **eqs 1-4** (Duval and Gaboriaud 2010; Moussa et al. 2015). Conformably to the above qualitative analysis of **Figure 1**, the isoelectric point of $SiNH_2$ NPs is located at pH~5. The nanometric length scale $1/\lambda_0$ (= 1 ± 0.3 nm) compares well with results obtained for latex particles of similar size (Duval et al. 2013). The absence of marked maximum for $|\mu|$ *versus* salt concentration in **Figure 1,** which contrasts with that evidenced for latex NPs (Duval et al. 2013), indicates that double layer polarization effects for $SiNH_2$ NPs are probably less significant than for latex NPs, which qualitatively agrees with the ρ_0 values of the former particle type at pH 7 that are *ca.* 10 times lower in magnitude than those derived for the latex NPs (Duval et al. 2013). Finally, the increase in $1/\lambda_0$ with pH suggests that the thickness and/or structure of the thin polyelectrolyte-like layer slightly changes with pH as a result of modification of the electrostatic interactions between neighboring -O^- or -NH_3^+ ionogenic surface groups, a feature evidenced for nanoparticulate dendrimers (Moussa et al. 2015). Following these conclusions, and exploiting the unexpected reversal in $SiNH_2$ NPs mobility at pH 5, the pH 7 and pH 3 conditions were selected for deciphering below the impacts of $SiNH_2$ NPs on cell electrokinetic properties (§3.2).

In order to ascertain that suspensions of $SiNH_2$ NPs remain stable against aggregation under conditions adopted for the experiments carried out in the presence of bacterial cells (*i.e.* pH 3 or 7, and 1 mM solution ionic strength), particle size measurements were performed by DLS at pH 3 and 7 as a function of salt concentration (**Figure 2**), as detailed in §2.3.1. In good agreement with independent TEM measurements (**Figure S1**), $SiNH_2$ NPs hydrodynamic diameter is 140 ± 10 nm at ionic strengths lower than 10 mM, regardless of pH. The NPs suspensions stability at pH 7 confirms the existence of (negative) electrostatic charges at the surface of $SiNH_2$ NPs (as independently evidenced by electrokinetics), which ensures the operability of repulsive interactions between particles and the establishment of a significant energy barrier they must overcome to form aggregates at such a pH. At larger solution ionic strengths (25 mM-150 mM) and pH 7, a bimodal distribution in particle size is obtained, which pinpoints the presence of particle aggregates with broad size distribution. The respective magnitude of the detected intensity peaks still denotes a predominant proportion of individual particles over that of aggregates (500 nm-700 nm in diameter). At 250 mM solution ionic strength, particles suspensions become unstable as particle size may then exceed micrometer scale and the contributions of aggregates to the overall size distributions becomes significant. Similar features are observed at pH 3. Given these elements, the stability of the $SiNH_2$ NPs suspensions against aggregation is ensured in 1 mM solution ionic strength both at pH 3 and 7 (the conditions adopted for electrokinetic analysis of binary NPs-cells system).

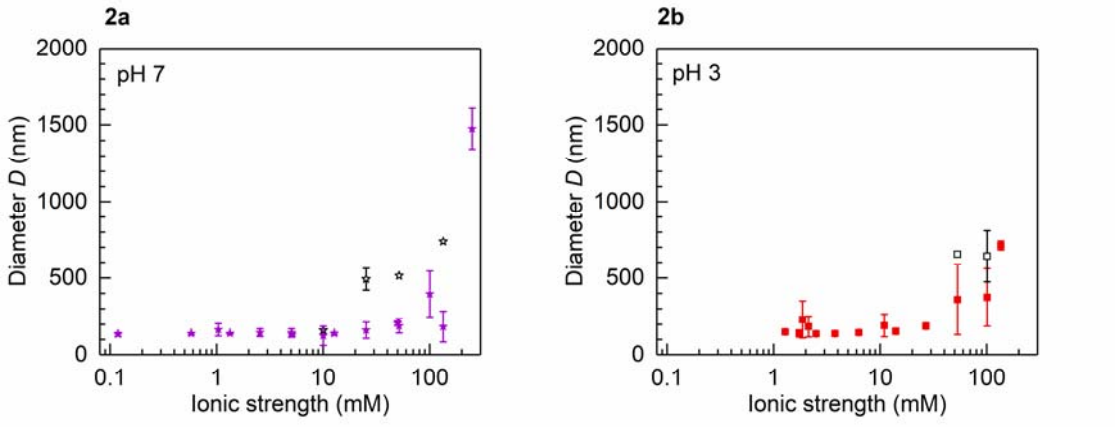

Figure 2: $SiNH_2$ NPs hydrodynamic diameter *D* at pH 7 (2a) and pH 3 (2b) as a function of solution ionic strength. Filled symbols correspond to the first mode detected in the number-size distributions obtained by DLS. Empty bullet points correspond to the second mode if applicable. Due to the contribution of protons to the overall solution ionic strength, there are no data points in panel b at 1 mM ionic strength after addition of KNO_3 electrolyte.

As our intention is to assess the electrokinetic cell features (in mixed cell-$SiNH_2$ NPs suspensions) as a function of NPs concentrations in solution, we further identified the range of $SiNH_2$ NPs concentration in line with constant $SiNH_2$ NPs electrophoretic mobility. Respecting the NPs concentrations window recommended by Malvern (NanoZS) and CAD (Zetaphoremeter IV apparatus) manufacturers, we found that the mobility of $SiNH_2$ NPs at pH 3 (pH 7, respectively) in 1 mM solution ionic strength is μ=2.1±0.6×10^{-8} m^{2}V^{-1}s^{-1} at 10^{-3} g L^{-1} (μ=-1.8±0.1×10^{-8} m^{2}V^{-1}s^{-1}, respectively) and μ=2.5±0.5×10^{-8} m^{2}V^{-1}s^{-1} at 10^{-2} g L^{-1} (μ=-2.0±0.4×10^{-8} m^{2}V^{-1}s^{-1}, respectively), as obtained with Zetaphoremeter IV equipment (CAD Instrumentations®). Measurements with Zetasizer NanoZS (Malvern) lead at pH 3 (pH 7, respectively) to μ=2.4±0.6×10^{-8} m^{2}V^{-1}s^{-1} at 10^{-2} g L^{-1} (μ=-1.9±0.7×10^{-8} m^{2}V^{-1}s^{-1}, respectively) and μ=3.0±0.7×10^{-8} m^{2}V^{-1}s^{-1} at 10^{-1} g L^{-1} (μ=-1.7±0.9×10^{-8} m^{2}V^{-1}s^{-1}, respectively). At fixed pH (3 or 7), within experimental error μ values therefore remain constant in the 10^{-3} g L^{-1} (or lower) to 10^{-2} g L^{-1} NPs concentration range: this NP concentration range is therefore adopted in §3.2 dedicated to the electrokinetic analysis of mixed NPs-bacteria suspensions using Zetaphoremeter IV equipment.

The electrophoretic mobility of the 3 different bacterial strains (nude, YeeJ or F-pili decorated cells, see §2.1) was measured as a function of solution ionic strength (1 mM to 250 mM at pH 3 and 7). Results are reported in **Figure 3**. As expected for bacterial cells, μ is negative for all strains at both pH conditions and the observed classical decrease of $|\mu|$ with increasing salt concentration refers to screening of the charges carried by cells envelopes (Duval and Gaboriaud 2010). Distinct electrokinetic cells responses are further observed depending on their respective surface phenotype. In detail, at pH 7 (**Figure 3a**) $|\mu|$ of the nude cells (E2152) is systematically higher than that measured for the F-pili- and YeeJ-decorated bacteria (E2302 and E2551, respectively). In addition, $|\mu|$ of E2302 (F-pili) and of E2551 (YeeJ) cells exhibit -within experimental error- identical electrokinetic behavior over the range of ionic strengths tested. The results displayed for E2152 (nude cells) and E2302 (F-pili bacteria) compare well with those previously reported by Francius et al. (2011), to which the reader is referred for details. The differences in mobility between the three strains primarily originate from modifications of the electrostatic cell surface features and cell drag forces as a result of the selective expressions of YeeJ and of F-pili protruding surface appendages. These modifications are addressed here from analysis of the data in **Figure 3** on the basis of **eqs 1-4** along the lines detailed above for

investigation of NPs electrokinetics (**Figure 1**), recalling that bacteria are paradigms of soft (bio)colloids (Duval and Gaboriaud 2010). The results provided in **Table 3** highlight that the density of charges distributed within the electrokinetically active peripheral zone of the nude bacteria at pH 7 is *ca.* two times higher than that pertaining to E2302 and E2551 cells. While the latter two bacterial strains are defined by similar ρ_o (~97±4 mM) and similar Brinkman lengths ($1/\lambda_o$~0.85 nm), their permeability to electroosmotic flow appears to be somewhat larger than that for nude cells ($1/\lambda_o$~0.5 nm). Surface appendages thus contribute here to slightly increase flow permeability (*i.e.* increase of $1/\lambda_o$) and to hydrodynamically screen the charges carried by the underlying supporting membrane, thereby reducing the density of the charges that are effectively probed by the tangential electroosmotic flow developed under electrophoretic conditions. Remarkably, within experimental error the electrokinetic properties of the three strains of interest are similar at pH 3 over the whole range of solution ionic strengths tested (**Figure 3b**), and the corresponding $|\mu|$ is systematically smaller than that measured at pH 7 due to expected protonation of the proteins and other moieties located at the bacterial cell surfaces. Overall, the respective magnitudes of $1/\lambda_o$ (= 0.7±0.2 nm, with no marked dependence on pH) and ρ_o values derived for the cells of interest at pH 7 and 3 correctly fit into the data compilation done by Duval and Gaboriaud from electrokinetic literature on Gram-negative bacteria (Duval and Gaboriaud 2010).

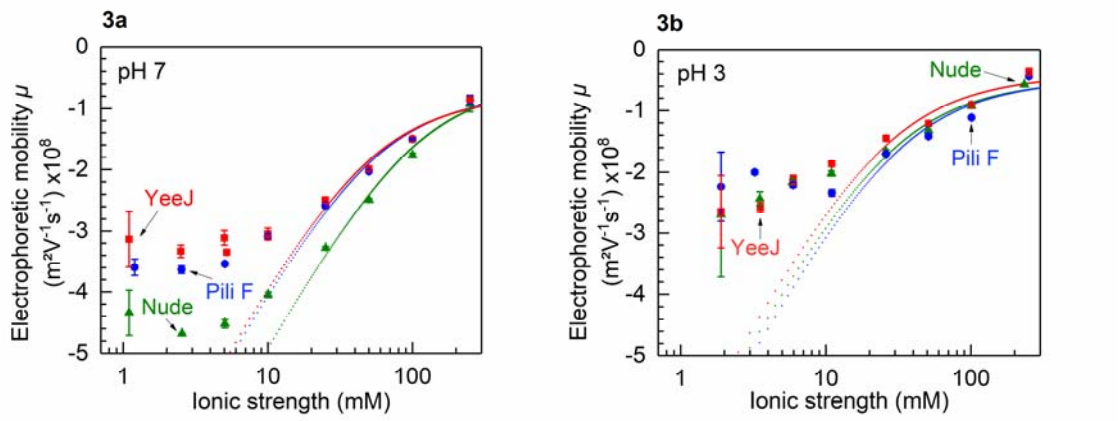

Figure 3: Electrophoretic mobility of the adopted bacterial strains (nude (E2152), F-pili (E2302) and YeeJ (E2551) cells, indicated) **at pH 7 (3a) and pH 3 (3b) as a function of solution ionic strength**. Symbols: experimental data. Dotted lines: theory (**eqs 1-4**). Due to the contribution of protons to the overall solution ionic strength, there are no data points in panel b at 1 mM ionic strength after addition of KNO_3 electrolyte.

3.2 Electrokinetics of mixed bacteria-NPs suspensions

The electrophoretic properties of the mixed bacteria-NPs suspensions (see methodology detailed in §2) are given in **Figure 4** in the forms of electrophoretic mobility distributions reported as a function of concentration of $SiNH_2$ NPs in solution at pH 7 and pH 3 for the different cell surface phenotypes considered in this work. For the sake of comparison, the mobility distributions featuring the electrokinetic properties of cells and NPs taken separately are further displayed in **Figure 4**. Accordingly, the first and last lines in each of the diagrams of **Figure 4** refers to the electrokinetic responses of $SiNH_2$ NPs and bacteria, respectively. The electrophoretic fingerprints of the cells and those of the $SiNH_2$ NPs in mixed NP-cells suspensions correspond to the mobility-plumes located at the left and right side of the diagrams in **Figure 4**, respectively. In **Figure 4**, the frequency reported

for a given class of electrophoretic mobility values μ (the width of each class is set here to 0.15×10^{-8} $m^2V^{-1}s^{-1}$ increment in μ) corresponds to the ratio between the number of particle trajectories detected at these selected μ and the total number of trajectories measured over the whole range of measured mobility values. As such, this frequency is systematically lower than unity. Traditionally, electropherograms display distributions of electrophoretic mobility in the form of frequency (of detected trajectories) *versus* μ (see *e.g.* Dague et al. 2006). The representation in **Figure 4** is nothing else than this, except that distributions are here reported as a function of NPs concentration in solution (*y*-axis) and that frequencies are scaled according to the color code detailed in **Figure 4**. The result is the establishment of 2D electrophoretic plumes of the cells and of the NPs whose deformation along the y-axis informs about NPs actions on microorganisms surface, as extensively discussed below.

At pH 7, in line with data in **Figure 3**, cells electrophoretic mobility ranges from -5 to -4×10^{-8} $m^2V^{-1}s^{-1}$ (E2152, nude cells), from -4 to -3×10^{-8} $m^2V^{-1}s^{-1}$ (E2551, YeeJ) and from -4 to -2.5 x 10^{-8} $m^2V^{-1}s^{-1}$ (E2302, F-pili decorated). The width and frequencies defining the mobility distributions of E2152 and E2551 cells remain basically unchanged upon increase of $SiNH_2$ NPs concentration up to 10^{-3} g L^{-1} (see the yellow core of the cells-associated plumes). With further increasing NPs concentration in solution, electrophoretic detection of the NPs becomes possible and their frequency of electrokinetic apparition increases noticeably, as judged from the color gradient in the down-to-top direction along the NPs-associated plumes in **Figures 4a** and **4b**. Concomitantly, there are lesser bacterial cells detected and their maximum frequency of electrokinetic apparition decreases from 0.2 to 0.05 with increasing NP concentrations from 10^{-3} g L^{-1} to 10^{-2} g L^{-1}. The most important conclusion at this stage is the absence of deformation of the cells-electrokinetic plume with increasing $SiNH_2$ NPs, which suggests that the electrohydrodynamic properties of E2152 and E2551 cells remain basically unaffected in the presence of $SiNH_2$ NPs. This is in line with the repulsive electrostatic interactions expected on the basis of the electrostatic properties of the negatively charged E2152/E2551 cells and $SiNH_2$ NPs as pictured in **Figure 3a** and **Figure 1**, respectively. Similar conclusions may be formulated for E2302 cells even though, qualitatively, the width of their mobility distributions tends to slightly increase with increasing $SiNH_2$ NPs from 0 to 10^{-2} g L^{-1}, resulting in an overlap of the cells- and NPs-plumes that is significantly more pronounced than for E2152 cells. This finding underpins that a fraction of E2302 cells are impacted *via e.g.* interactions of their long protruding pili with NPs, a mechanism that can bypass the repulsive energy barrier that is otherwise required for E2152 cells and NPs to get into contact (van Loosdrecht et al. 1990). This feature would obviously require further investigation at the proper F-pili spatial scale *via e.g.* dedicated AFM-based investigations. Within the limits of detection, there are no obvious sign of changes of the native NP electrokinetic signal in the presence of bacteria at pH 7, irrespective of the cells surface phenotype considered.

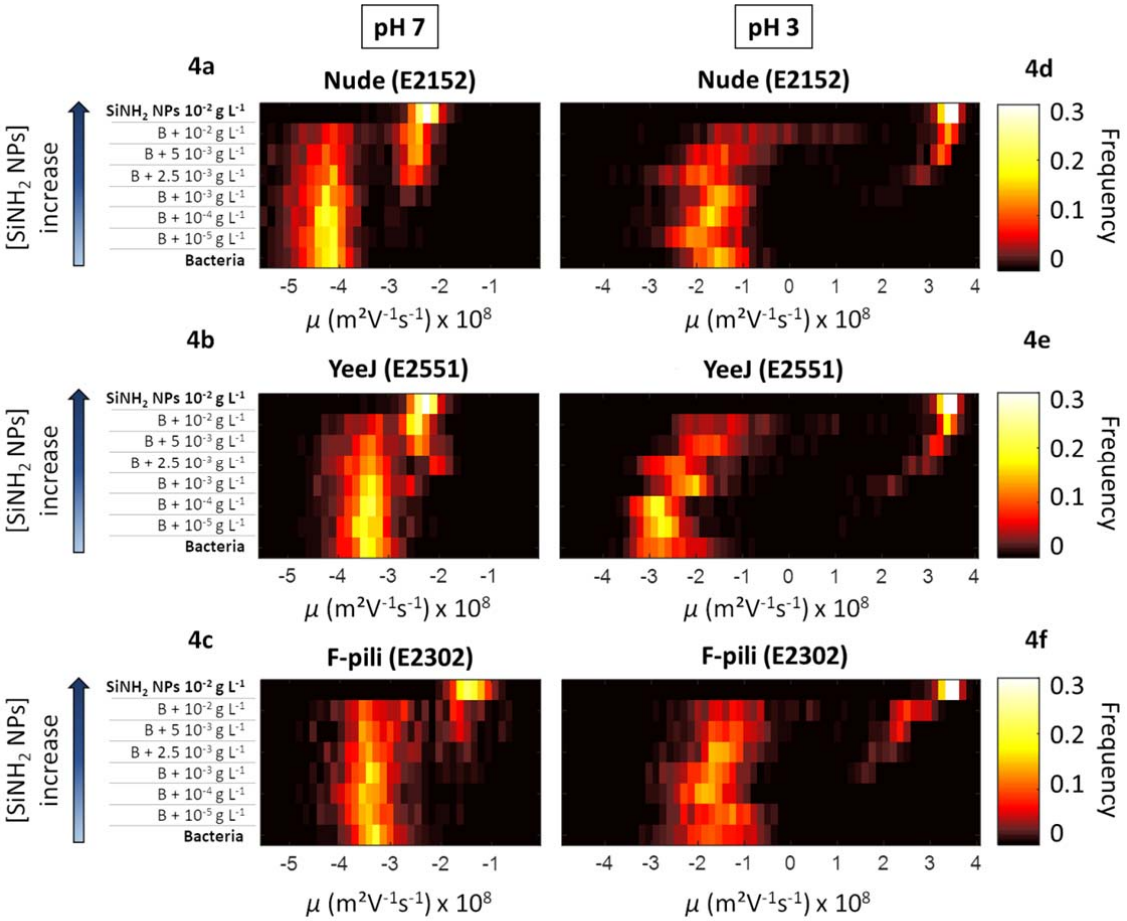

Figure 4: Electrophoretic fingerprints of mixed bacteria-$SiNH_2$ NPs suspensions at pH 7 and pH 3 (indicated) as a function of $SiNH_2$ NPs concentration in solution for the three cell surface phenotypes of interest (indicated). Solution ionic strength: 1 mM at pH 7 and 2 mM at pH 3. See text for details (§2 and §3.2). 'B' stands for bacteria.

At pH 3 (**Figures 4d, e, f**), the situation dramatically differs from that discussed at pH 7. Indeed, the mobility distributions pertaining to the bacterial cells and/or to the $SiNH_2$ NPs, set under mixed conditions, are now significantly impacted with increasing NPs concentration in solution. The associated deformations of the cells- and/or NPs-electrokinetic plumes further differ according to the cell surface phenotype considered. In detail, starting with the case of E2551 bacteria (YeeJ-decorated cells, **Figure 4e**), the signal stemming from bacteria is clearly shifted to lesser negative mobility values in the presence of $SiNH_2$ NPs and the more so as the NPs concentration increases. The corresponding width of mobility distribution further increases and its extremes are shifted to more positive values. This distortion of the cells-electrokinetic plume compounds the shift of the NPs-associated electrokinetic fingerprints to more positive values with increasing NPs concentration in solution. These results indicate that electrostatic attractions operating between positively charged $SiNH_2$ NPs (**Figure 1**) and negatively charged E2551 cells (**Figure 3b**) at pH 3 induce significant changes of the surface features of **both** bacteria and NPs. More specifically, a fraction of NPs likely adsorbs at the cells surface to an extent that depends on electrostatics (favourable at pH 3) and on their chemical affinity to cell surface biocompounds (YeeJ proteins or other molecules like lipopolysaccharides). Other possible NPs action mode includes cell surface abrasion and subsequent

removal of charged bio-residues originally anchored at the cell membrane (Shrivastava et al. 2007). As a result, the effective charge density of the so-modified cell envelope probed by electrokinetics becomes less negative, in line with the cells-plume features given in **Figures 4e**. In addition, bacterial cells under stress conditions may excrete biomolecules (*e.g.* proteins, metabolites, exopolysaccharides). The latter in turn can modify the surface properties of the external agents at the origin of the stress (here the $SiNH_2$ NPs) (Kimkes and Heinemann 2018; Majdalani et al. 2005), minimize the impacts cells undergo and/or diminish the long-scale interactions that cells experience with these stressors (Zeyons et al. 2009). These biomolecules may further be released following NP-mediated cell surface abrasion invoked above and/or cleavage of cellular surface material following holes formation at the membrane. Such biotic retroaction processes would lead to a (negatively charged) bio-corona acquisition by NPs, and thus to a decrease of the net surface charge of the $SiNH_2$ NPs (Sheng et al. 2005; Zeyons et al. 2009). This expectation agrees with the trend in **Figure 4e** and with the aforementioned changes in $SiNH_2$ NPs electrokinetic plume. Obviously, the higher the $SiNH_2$ NPs content in solution (at fixed cells concentration), the lower the modification of their surface upon interaction with cells and/or with excreted cells biocomponents, the easier is their electrokinetic detection in mixed cell-NPs suspension and, concomitantly, the lesser efficient becomes the electrophoretic tracking of cells. This argument explains the decrease (increase, respectively) of the frequency maximum in mobility distributions pertaining to the cells (NPs, respectively) upon increasing $SiNH_2$ NPs concentration. This conclusion is supported by the colour scale gradient upon moving along the deformed cell- and NPs-electrokinetic plumes.

Qualitatively, the modulations discussed above for the E2551/$SiNH_2$ NPs electrokinetic diagram at pH 3 are also observed for the mixed E2152/$SiNH_2$ NPs at this pH (**Figure 4d**). However, the distortions of the $SiNH_2$ NPs- and E2152-plumes take place at larger NPs concentrations, *i.e.* 2.5×10^{-3} g L^{-1} and 10^{-2} g L^{-1}, respectively, instead of 10^{-3} g L^{-1} and 5×10^{-3} g L^{-1} for the E2551/NPs system. This suggests that the resistance of the nude E2152 bacteria against NPs action is more efficient than that of YeeJ-decorated cells. Possibly, the protusion of YeeJ proteic islands over the cell surface facilitates non-specific electrostatic attractions with incoming NPs, as anticipated from theory by Duval *et al*. on interactions between rough surfaces (Duval et al. 2004). YeeJ proteins can also feature shorter-range specific interactions with $SiNH_2$ NPs. In both scenarios, YeeJ proteins promote contacts between cells and $SiNH_2$ NPs and, therewith, NPs-mediated modifications of the overall cell electrosurface characteristics. Finally, it is found that the situation for E2302/$SiNH_2$ NPs (**Figure 4f**) is intermediate between that for E2551/$SiNH_2$ NPs and E2152/$SiNH_2$ NPs systems. Indeed, while the deformation of the E2302 electrokinetic plume better compares with that obtained for the nude E2152 bacteria (**Figure 4d**), the marked modulation of the $SiNH_2$ NPs signal in the presence of E2302 cells is qualitatively more similar to that of $SiNH_2$ NPs in presence of E2551 cells (**Figure 4e**). Further comparison between **Figure 4e** and **Figure 4f** reveals that modifications of the $SiNH_2$ NPs surface properties with increasing $SiNH_2$ NPs concentration in NPs-cells mixtures are more significant in presence of E2302 cells than they are with E2551 cells. This conclusion is inferred from the corresponding shift in NPs electrophoretic mobility distribution to lesser positive values at fixed NPs concentration. Addressing the complex molecular processes that govern the modifications of the cells and NPs surface properties would obviously require reasoning beyond the electrokinetics framework and ask for integration of *e.g.* genomic/transcriptomic or micro-spectroscopy data in the analysis, which is not the scope of the current study. Instead, we demonstrate that simple electrophoretic methods may already help in detecting rapidly cells that are impacted by NPs, and identify some conditions where such effects are at stake. Altogether, **Figure 4** evidences (i) the role of electrostatics in mediating NPs-cells interactions, (ii) the heterogeneous response of the cells to NPs exposition (as reflected by changes in mobility distribution width), and (iii) the differentiated

roles played by cells surface bio-compounds in promoting or not NPs action. In the next section, we provide AFM images of individual cells exposed to $SiNH_2$ NPs as an additional support for the trends given in **Figure 4**, recalling that electrokinetic measurements refer to averages of electrohydrodynamic properties over the whole assembly of cells in solution.

3.3 Bacterial cell surface imaging and roughness evaluation

TEM is commonly adopted for imaging biological samples (El Badawy et al. 2011; Silva et al. 2014). However, the required sample preparation protocol, which involves sample drying, may lead to degradation of the native biosurface structures (Hardij et al. 2013). AFM measurements in liquid environment offer an option for avoiding such artefacts (Beaussart et al. 2018b; Bolshakova et al. 2004; Dufrêne 2008; Jandt 2001). **Figure 5** collects typical AFM Peak Force images obtained for the three bacterial strains of interest, E2152, E2551 and E2302 before and after exposure to $SiNH_2$ NPs at pH 7 and pH 3.

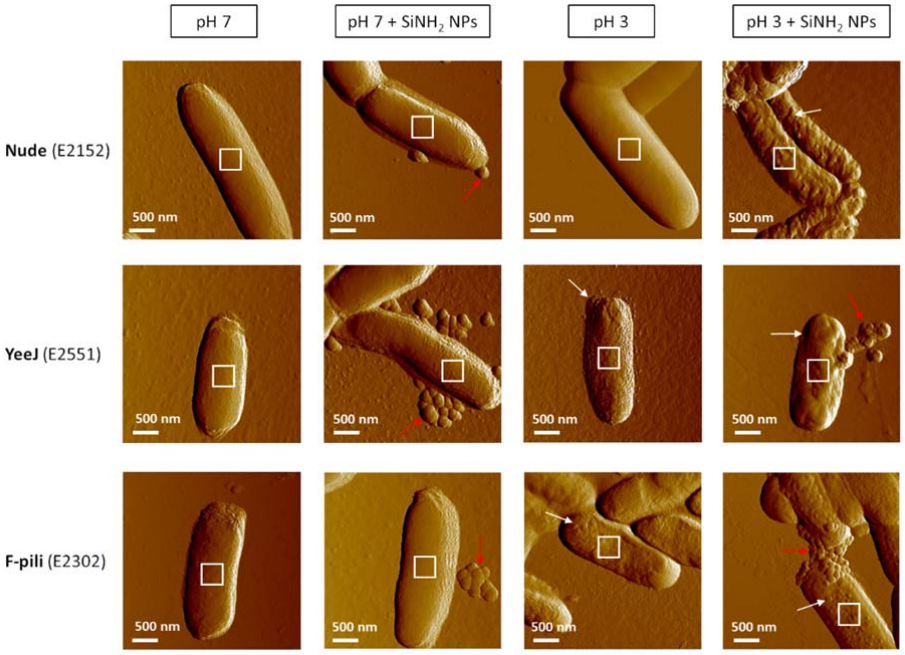

Figure 5: AFM peak force error images (3.5 µm × 3.5 µm, 256 pixels × 256 pixels) taken in liquid for E2152, E2551 and E2302 bacteria (indicated) at pH 7 and 3 (indicated) prior to and after incubation with NPs (see details in §2). Red arrows correspond to NPs, white arrows to asperities or depressions, white squares define 400 nm × 400 nm spatial regions where cell surface roughness features were evaluated.

The AFM cell pictures obtained in the absence of $SiNH_2$ NPs at pH 7 (left column, **Figure 5**) display normal bacterial morphologies with aspects that agree well with those detailed in previous reports (Beloin et al. 2010; Francius et al. 2011). In particular, identification of YeeJ and pili structures at the surfaces of E2551 and E2302 is not possible from AFM imaging under liquid conditions as argued elsewhere (Francius et al. 2011). Cell surface imaging in air allows however visualization of the long surface appendages like pili (**Figure S2** in Supplementary Material). In the presence of $SiNH_2$ NPs (2^{nd} column from the left, **Figure 5**), cell envelopes imaged at pH 7 do not suffer from marked asperities or depressions even though individual $SiNH_2$ NPs or aggregates may be found in the close vicinity of the cells and/or at their surface. The corresponding AFM images contrast with those obtained at pH 3 in the presence of $SiNH_2$ NPs (right column in **Figure 5**). Under such conditions, nude E2152 cell

surfaces appear wrinkled, YeeJ-decorated E2551 cells anomalously disrupted with pronounced inflammatory points, and E2302 cells (with F-pili) significantly blistered all over their surface envelope that is in further intimate contact with apparently cohesive $SiNH_2$ NPs clusters. Modifications of E2302 and E2551 surface morphologies and topographies are also -to a lesser extent- caused by the acidic pH environment, as revealed by AFM images on selected cells obtained at pH 3 in the absence of $SiNH_2$ NPs (third column from left in **Figure 5**). Images of certain YeeJ-decorated cells collected at pH 3 without $SiNH_2$ NPs (not shown here) indicate the presence of spheroids with *ca.* 70 nm diameter in the vicinity of their surface. The origin and nature of these entities remain difficult to establish, *e.g.* they could identify with outer membrane vesicles (OMVs). The latter may originate from the constitutively expressed YeeJ, which slightly perturbs outer membrane structure and favours OMVs production (McBroom and Kuehn 2007) and/or acidic pH condition may induce outer membrane structure modifications and lead to a release of (aggregated) YeeJ proteins. Altogether, the $SiNH_2$ NPs-induced changes in cell surface integrity recall those identified on *E. coli* bacteria (MRE 162 strain) exposed to negatively-charged modified SiO_2 NPs (diameter < 80 nm) or to positively-charged functionalized SiO_2 NPs (diameter *ca.* 100 nm) synthetized according to Hartlen protocol (Hartlen et al. 2008; Mathelié-Guinlet et al. 2018). Qualitatively, the electrokinetic fingerprints of mixed NPs-cells suspensions displayed in **Figure 4** at pH 7 and 3 well conform to the qualitative presence or absence of marked cell surface alterations pictured in **Figure 5.** The highly heterogeneous cell surface properties identified by AFM at the single cell level in the presence of $SiNH_2$ NPs echo the dispersity of the mobility distributions symptomatic of the heterogeneous cells response examined at the population scale.

Various procedures are reported in the literature to quantify cells surface roughness, and they differ according to the mode of evaluation of the reference surface, *e.g.* using least-squares, multinomial or arithmetic mean regression (Chen et al. 1999). Once determined, this reference surface is subtracted from the initial raw image and the sample surface roughness can then be estimated on the basis of the distribution in local height variations. These methods however suffer from the non-unicity of the reference surface whose characteristics inherently depend on factors like sampling length and sampling location (Chen et al. 1999). It is therefore required to resort to frequency-based sampling of cells surface heterogeneities, as done within the framework of wavelet analysis (Chen et al. 1999) or Gaussian filtering (Geusebroek et al. 2003) of images. In this work, a Gaussian filter with standard deviation σ_1 ranging from 0.4 to unity was applied to 400 nm × 400 nm AFM images of bacteria (**Figure 5**). The resulting images were subsequently subtracted from the initial AFM images, thus making possible the estimation of the relevant distribution of heights counted from the corresponding basal cell topography reference. Typical examples are given in **Figure 6**. The height distributions were then successfully fitted according to a normal distribution law (centered at the maximal height value) defined by a standard deviation, hereafter denoted as σ_2, that varies linearly with σ_1. The (dimensionless) slope (denoted as ω) of the obtained σ_2 *versus* σ_1 linear plots reflects the searched cell surface roughness, with a perfectly smooth surface corresponding to $\omega = 0$. **Figures S3**, **S4** and **S5** in Supplementary Material illustrate the different steps of this procedure we followed for evaluation of cells surface roughness. The ω proxies for cell surface roughness, as derived under the conditions of **Figure 5**, are reported in **Table 4.**

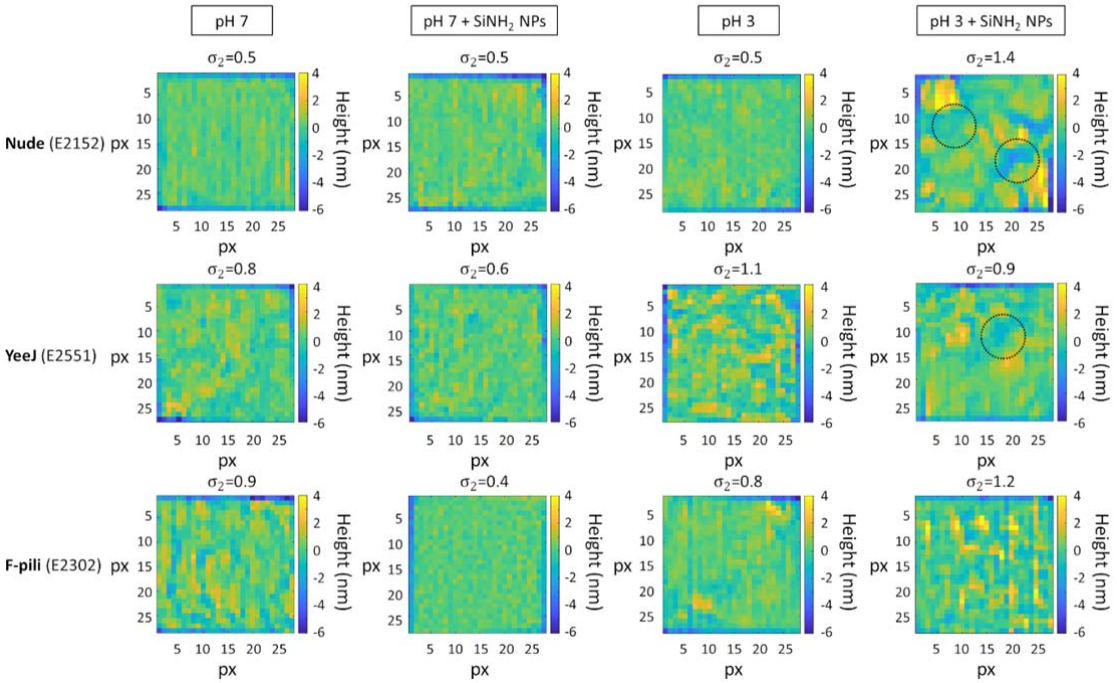

Figure 6: Illustrative spatial mapping (400 nm × 400 nm, 28 pixels × 28 pixels) of sample heights derived after application of a Gaussian filter (here, standard deviation σ_1=1) and subtraction from the corresponding raw images. Locations of surface areas where roughness analysis was conducted are provided in **Figure 5** for illustration (white squares therein). Bacterial surfaces were imaged at pH 7 and 3 in the presence of 10^{-3} g L^{-1} $SiNH_2$ NPs (indicated). σ_2 corresponds to the standard deviation in height distribution successfully fitted according to a normal distribution law. The black dotted circles are defined by a radius that is equivalent to that of a single NP, and they are positioned at cell surface areas featuring lateral heterogeneities with dimensions reminiscent of NP fingerprints. 'px' stands for pixel. Lines of blue pixels positioned at the image borders correspond to side effects in Gaussian filtration procedure and these pixels were thus not considered for evaluation of σ_2.

For the nude (E2152) strain imaged at pH 7 in the absence of NPs, σ_2 evaluated at σ_1=1 is 0.5 (**Figure 6**). For the YeeJ (E2551) and F-pili (E2302) strains, σ_2 reaches larger values (0.8 or 0.9 at σ_1=1), which is in agreement with the presence of peripheral surface appendages and with the so-rendered rougher cell walls. The presence of $SiNH_2$ NPs tends to 'smooth' the surface of YeeJ and F-pili bacteria at pH 7 (σ_2~0.4-0.6 at σ_1=1) and the roughness associated with the presence of the parietal structures then becomes less pronounced. Acidic pH environment does not seem to significantly affect the roughness of bacterial surface evaluated at pH 7, except for YeeJ cell type. However, the presence of $SiNH_2$ NPs at pH 3 leads to the formation of craters or depressions (-2 nm to 0 nm in height) for the nude (E2152) and YeeJ (E2551) strains -which possibly corresponds to NP fingerprints (**Figure 6**)- and to surface islands whose size is significantly larger than that observed in the absence of NPs. Although distinguishable artefacts remain after application of the Gaussian filter to images of F-pili (E2302) at pH 3 in the presence of NPs, σ_2 estimated at σ_1=1 under such conditions is significantly larger than that obtained at pH 3 in the absence of NPs. The above observations are based on height mappings collected on a given bacterial cell and discussed at a specific frequency-filtration defined by σ_1=1. To provide a hint of the inherent heterogeneities in cell damages caused by NPs, we discuss below the ω-results obtained from analysis of 3 to 7 distinct cells (**Table 4**). These results reflect the outcomes of the image filtration procedure over a larger range of selected σ_1 values (0.4 to 1).

Concerning nude (E2152) bacteria, ω is of the same order of magnitude at pH 7 and at pH 3 in the absence of $SiNH_2$ NPs, which is in line with qualitative observations of **Figure 5**. For the YeeJ (E2551) strain, ω significantly increases from pH 7 (1.23) to pH 3 (1.96), thus highlighting the impact of an acidic environment on cell surface morphology, as invoked from analysis of **Figure 5**. For F-pili (E2302) bacteria, acidic pH condition seems to induce a 'smoothing' of the cells surface (1.15 instead of 1.43 at pH 7) but firm conclusions are difficult to derive due to lack of statistics (see reasons in caption **Table 4**). Furthermore, the presence of $SiNH_2$ NPs at pH 3 magnifies the roughness of F-pili (E2302) cells surface estimated in the absence of NPs. Unlike E2302 cells at pH 7, ω pertaining to E2152 and E2551 cells is not significantly impacted by the presence of $SiNH_2$ NPs. At pH 3, ω for E2152 cells is *ca.* two times higher in the presence of $SiNH_2$ NPs, which conforms to the disrupted cell surface featured in **Figure 5**. The pronounced depressions observed all over E2152 cell surfaces possibly result from contacts with $SiNH_2$ NPs as their diameter (*ca.* 150 nm) qualitatively compares with that of $SiNH_2$ NPs (**Figures 5**, **6**). These lesions are the result of an alteration of the bacterial membrane integrity and potentially to a disruption of the peptidoglycan layer (Mathelié-Guinlet et al. 2018). For the YeeJ (E2551) strain, ω at pH 3 is lower in presence of NPs, consistent with the apparent cell surface flattening observed in **Figures 5 and 6**. This is possibly due to the presence of the spheroids with *ca.* 70 nm diameter observed at pH 3 in the absence of NPs by AFM for YeeJ (E2551) strain. These spheroids may correspond to outer membrane vesicles and their presence at the cell surface as well as their very production mechanism (budding of the outer membrane) likely result in the formation of membrane defects, reflected by an increase in surface roughness at pH 3 as compared to pH 7. In turn, such so-rendered fragile membrane could undergo an efficient abrasion by the NPs, leading to smoothing of the cell envelope. Another scenario can be proposed by examining the way YeeJ proteins are anchored at the outer membrane. Indeed, YeeJ proteins are composed of several domains: a LysM domain which is anchored in the peptidoglycan, a β-barrel domain embedded in the outer membrane and a passenger domain on the exposed C-terminal region of the protein (Martinez-Gil et al. 2017). The only passenger domain can be cleaved from the bacterial surface. Upon NPs action, YeeJ could undergo an abrasion of the exposed passenger domain, leading to a smoothing of the cell envelope, while the LyM and β-barrel domains would stabilise the cell wall, thereby preventing further damage of the outer membrane (such mechanism could hold both at pH 3 and 7). Obviously, analysis of such scenario would require further investigations with use of dedicated micro-spectroscopies. **Table 4** suggests that YeeJ-cells E2551 are the most affected strain when lowering pH from 7 to 3 in the absence of $SiNH_2$ NPs. In parallel, **Figure 4** evidences that this strain is the one among the three investigated for which the shift in electrophoretic mobility is the most significant at pH 3 with increasing $SiNH_2$ NPs concentration. These observations underpin the pronounced sensitivity of E2551 to external stressors (pH and NPs conditions) and the propensity of these cells to be strongly affected when these stressors are combined (cocktail effect).

4. Conclusions

In this study, we show that electrophoresis of mixed suspensions of bacteria and NPs is a suitable method for screening the impacts of NPs on cell charge density, cell envelope integrity and/or peripheral structure, which translates into detectable modifications of the electrohydrodynamic cell fingerprints. The existence of favorable attractive interactions between NPs and cells -and of the subsequent changes in the physicochemical properties of the cell surfaces following their contacts and collisions with NPs- can be rapidly 'read' from inspection of the cells and NPs mobility distributions, *e.g.* measured as a function of NPs concentration and pH. In particular, the associated deformation of the electrokinetic plumes pertaining to cells and NPs can provide information not only on the critical NPs concentration marking the onset of significant NPs action, but also on

possible biological retroaction processes leading to alterations of NPs surface properties. The demonstration is based on measurements performed on genetically engineered *E. coli* cells defined by distinct surface phenotypes and on functionalized silica NPs (65 nm radius) whose respective electrokinetic characterizations are given here in terms of relevant soft surface electrokinetic concepts instead of meaningless zeta potential parameter. The analysis clearly highlights the role of electrostatics and of cell surface bio-compounds in mediating cells-NPs interactions and ensuing NPs-mediated deleterious effects on bio-surface. Electrokinetic data are further qualitatively supported by AFM cell surface imaging, thereby featuring multiscale heterogeneities in cells response to NPs, from the cell (*via* AFM) to the population (*via* electrokinetics) organization levels. Altogether, this study demonstrates the potential of electrokinetics to probe the precursory NPs-cells interactions that initiate adverse impacts of NPs on living organisms. This work further paves the way for preliminary electrokinetics-based assessment of NPs toxicity to microorganisms and for rapid pre-screening of eco-friendly nanoparticulate materials.

5. Supplementary material

TEM picture of $SiNH_2$ NPs (**Figure S1**), AFM peak force error images, taken in air, for F-pili (E2302) bacteria at pH 7 (**Figure S2**), and illustration of the various steps followed for the evaluation of cells surface roughness for YeeJ (E2551) strain at pH 7, for nude (E2152) strain at pH 3 in the presence of $SiNH_2$ NPs (10^{-3} g L^{-1}) and for F-pili (E2302) strain at pH 3 in the presence of $SiNH_2$ NPs (10^{-3} g L^{-1}) (**Figures S3**, **S4** and **S5**, respectively) are provided as supplementary material.

6. Conflicts of interest

The authors declare no conflicts of interest.

7. Acknowledgements

This research did not receive any specific funding.

References

El Badawy, A.M., Silva, R.G., Morris, B., Scheckel, K.G., Suidan, M.T., Tolaymat, T.M., 2011. Surface charge-dependent toxicity of silver nanoparticles. *Environ. Sci. Technol.* **45**, 283–287. https://doi.org/10.1021/es1034188

Beaussart, A., Beloin, C., Ghigo, J.-M., Chapot-Chartier, M.-P., Kulakauskas, S., Duval, J.F.L., 2018a. Probing the influence of cell surface polysaccharides on nanodendrimer binding to Gram-negative and Gram-positive bacteria using single-nanoparticle force spectroscopy. *Nanoscale* **10**, 12743–12753. https://doi.org/10.1039/c8nr01766b

Beaussart, A., Caillet, C., Bihannic, I., Zimmermann, R., Duval, J.F.L., 2018b. Remarkable reversal of electrostatic interaction forces on zwitterionic soft nanointerfaces in a monovalent aqueous electrolyte: An AFM study at the single nanoparticle level. *Nanoscale* **10**, 3181–3190. https://doi.org/10.1039/c7nr07976a

Beddoes, C.M., Case, C.P., Briscoe, W.H., 2015. Understanding nanoparticle cellular entry: A physicochemical perspective. *Adv. Colloid Interface Sci.* **218**, 48–68. https://doi.org/10.1016/j.cis.2015.01.007

Beloin, C., Roux, A., Ghigo, J., 2010. Escherichia coli biofilms. *Curr Top Microbiol Immunol* **322**, 249–389. https://doi.org/10.1007/978-3-540-75418-3_12

Beveridge, T.J., Graham, L.L., 1991. Surface layers of bacteria. *Microbiol. Rev.* **55**, 684–705.

Bolshakova, A. V., Kiselyova, O.I., Yaminsky, I. V., 2004. Microbial surfaces investigated using atomic force microscopy. *Biotechnol. Prog.* **20**, 1615–1622. https://doi.org/10.1021/bp049742c

Brayner, R., Ferrari-Iliou, R., Brivois, N., Djediat, S., Benedetti, M.F., Fiévet, F., 2006. Toxicological impact studies based on Escherichia coli bacteria in ultrafine ZnO nanoparticles colloidal medium. *Nano Lett.* **6**, 866–870. https://doi.org/10.1021/nl052326h

Chai, H., Yao, J., Sun, J., Zhang, C., Liu, W., Zhu, M., Ceccanti, B., 2015. The effect of metal oxide nanoparticles on functional bacteria and metabolic profiles in agricultural soil. *Bull. Environ. Contam. Toxicol.* **94**, 490–495. https://doi.org/10.1007/s00128-015-1485-9

Chaveroche, M.K., Ghigo, J.M., D'Enfert, C., 2000. A rapid method for efficient gene replacement in the filamentous fungus Aspergillus nidulans. *Nucleic Acids Res.* **28**. https://doi.org/10.1093/nar/28.22.e97

Chen, Q., Yang, S., Li, Z., 1999. Surface roughness evaluation by using wavelets analysis. *Precis. Eng.* **23**, 209–212. https://doi.org/https://doi.org/10.1016/S0141-6359(99)00013-6

Choi, O., Yu, C.-P., Esteban Fernández, G., Hu, Z., 2010. Interactions of nanosilver with Escherichia coli cells in planktonic and biofilm cultures. *Water Res.* **44**, 6095–6103. https://doi.org/10.1016/j.watres.2010.06.069

Colvin, V.L., 2004. The potential environmental impact of engineered nanomaterials. *Nat. Biotechnol.* **22**, 760–760. https://doi.org/10.1038/nbt0604-760c

Costa, T.R.D., Ilangovan, A., Ukleja, M., Redzej, A., Santini, J.M., Smith, T.K., Egelman, E.H., Waksman, G., 2016. Structure of the bacterial sex F pilus reveals an assembly of a stoichiometric protein-phospholipid complex. *Cell* **166**, 1436–1444. https://doi.org/10.1016/j.cell.2016.08.025

Crucho, C.I.C., Baleizão, C., Farinha, J.P.S., 2017. Functional group coverage and conversion quantification in nanostructured silica by 1 H NMR. *Anal. Chem.* **89**, 681–687. https://doi.org/10.1021/acs.analchem.6b03117

Dague, E., Duval, J., Jorand, F., Thomas, F., Gaboriaud, F., 2006. Probing surface structures of Shewanella spp. by microelectrophoresis. *Biophys. J.* **90**, 2612–2621. https://doi.org/10.1529/biophysj.105.068205

Delgado, A. V., González-Caballero, F., Hunter, R.J., Koopal, L.K., Lyklema, J., 2005. Measurement and interpretation of electrokinetic phenomena (IUPAC Technical Report). *Pure Appl. Chem.* **77**, 1753–1805. https://doi.org/10.1351/pac200577101753

Diallo, M.S., Christie, S., Swaminathan, P., Balogh, L., Shi, X., Um, W., Papelis, C., Iii, W.A.G., Johnson, J.H., 2004. Dendritic chelating agents. 1. Cu(II) binding to ethylene diamine core Poly(amidoamine) dendrimers in aqueous solutions. *Langmuir* **20**, 2640–2651. https://doi.org/10.1021/la036108k

Dubey, R.V., Maheshwari, D.K., 1999. A textbook of microbiology. S. Chand Publishing.

Dufrêne, Y.F., 2008. Towards nanomicrobiology using atomic force microscopy. *Nat. Rev. Microbiol.* **6**, 674–680. https://doi.org/10.1038/nrmicro1948

Duval, J.F.L., 2017. Chemodynamics of metal ion complexation by charged nanoparticles: A dimensionless rationale for soft, core-shell and hard particle types. *Phys. Chem. Chem. Phys.* **19**, 11802–11815. https://doi.org/10.1039/c7cp01750b

Duval, J.F.L., Farinha, J.P.S., Pinheiro, J.P., 2013. Impact of electrostatics on the chemodynamics of highly charged metal−polymer nanoparticle complexes. *Langmuir* **29**, 13821–13835. https://doi.org/10.1021/la403106m

800 Duval, J.F.L., Gaboriaud, F., 2010. Progress in electrohydrodynamics of soft microbial particle
801 interphases. *Curr. Opin. Colloid Interface Sci.* **15**, 184–195.
802 https://doi.org/10.1016/j.cocis.2009.12.002

803 Duval, J.F.L., Leermakers, F.A.M., Van Leeuwen, H.P., 2004. Electrostatic interactions between double
804 layers: Influence of surface roughness, regulation, and chemical heterogeneities. *Langmuir* **20**,
805 5052–5065. https://doi.org/10.1021/la030404f

806 Duval, J.F.L., Ohshima, H., 2006. Electrophoresis of diffuse soft particles. *Langmuir* **22**, 3533–3546.
807 https://doi.org/10.1021/la0528293

808 Flemming, H.C., Wingender, J., Szewzyk, U., Steinberg, P., Rice, S.A., Kjelleberg, S., 2016. Biofilms: An
809 emergent form of bacterial life. *Nat. Rev. Microbiol.* **14**, 563–575.
810 https://doi.org/10.1038/nrmicro.2016.94

811 Francius, G., Polyakov, P., Merlin, J., Abe, Y., Ghigo, J.M., Merlin, C., Beloin, C., Duval, J.F.L., 2011.
812 Bacterial surface appendages strongly impact nanomechanical and electrokinetic properties of
813 escherichia coli cells subjected to osmotic stress. *PLoS One* **6: e20066**.
814 https://doi.org/10.1371/journal.pone.0020066

815 Geusebroek, J., Smeulders, A.W.M., van de Weijer, J., 2003. Fast anisotropic gauss filtering **12**, 938–
816 943.

817 Hardij, J., Cecchet, F., Berquand, A., Gheldof, D., Chatelain, C., Mullier, F., Chatelain, B., Hardij, J.,
818 Cecchet, F., Berquand, A., Gheldof, D., Chatelain, C., 2013. Characterisation of tissue factor-
819 bearing extracellular vesicles with AFM: Comparison of air-tapping-mode AFM and liquid Peak
820 Force AFM. *J. Extracell. Vesicles* **3078**. https://doi.org/10.3402/jev.v2i0.21045

821 Hartlen, K.D., Athanasopoulos, A.P.T., Kitaev, V., 2008. Facile preparation of highly monodisperse
822 small silica spheres (15 to >200 nm) suitable for colloidal templating and formation of ordered
823 arrays. *Langmuir* **24**, 1714–1720. https://doi.org/10.1021/la7025285

824 Hayden, S.C., Zhao, G., Saha, K., Phillips, R.L., Li, X., Miranda, O.R., Rotello, V.M., El-Sayed, M.A.,
825 Schmidt-Krey, I., Bunz, U.H.F., 2012. Aggregation and interaction of cationic nanoparticles on
826 bacterial surfaces. *J. Am. Chem. Soc.* **134**, 6920–6923. https://doi.org/10.1021/ja301167y

827 Hill, R.J., Saville, D.A., Russel, W.B., 2003. Electrophoresis of spherical polymer-coated colloidal
828 particles. *J. Colloid Interface Sci.* **258**, 56–74. https://doi.org/10.1016/S0021-9797(02)00043-7

829 Huang, Z., Zheng, X., Yan, D., Yin, G., Liao, X., Kang, Y., Yao, Y., Huang, D., Hao, B., 2008. Toxicological
830 effect of ZnO nanoparticles based on bacteria. *Langmuir* **24**, 4140–4144.
831 https://doi.org/10.1021/la7035949

832 Ikuma, K., Decho, A.W., Lau, B.L.T., 2015. When nanoparticles meet biofilms-interactions guiding the
833 environmental fate and accumulation of nanoparticles. *Front. Microbiol.* **6**, 1–6.
834 https://doi.org/10.3389/fmicb.2015.00591

835 Ingale, A.G., Chaudhari, A.N., 2013. Biogenic synthesis of nanoparticles and potential applications : an
836 eco-friendly approach. *Nanomedecine Nanotechnol.* **4**. https://doi.org/10.4172/2157-
837 7439.1000165

838 Jacobson, K.H., Gunsolus, I.L., Kuech, T.R., Troiano, J.M., Melby, E.S., Lohse, S.E., Hu, D., Chrisler,
839 W.B., Murphy, C.J., Orr, G., Geiger, F.M., Haynes, C.L., Pedersen, J.A., 2015. Lipopolysaccharide
840 density and structure govern the extent and distance of nanoparticle interaction with actual
841 and model bacterial outer membranes. *Environ. Sci. Technol.* **49**, 10642–10650.
842 https://doi.org/10.1021/acs.est.5b01841

Jandt, K.D., 2001. Atomic force microscopy of biomaterials surfaces and interfaces. *Surf. Sci.* **491**, 303–332. https://doi.org/10.1016/S0039-6028(01)01296-1

Jiang, W., Yang, K., Vachet, R.W., Xing, B., 2010. Interaction between oxide nanoparticles and biomolecules of the bacterial cell envelope as examined by infrared spectroscopy. *Langmuir* **26**, 18071–18077. https://doi.org/10.1021/la103738e

Ju-Nam, Y., Lead, J.R., 2008. Manufactured nanoparticles: An overview of their chemistry, interactions and potential environmental implications. *Sci. Total Environ.* **400**, 396–414. https://doi.org/10.1016/j.scitotenv.2008.06.042

Kimkes, T.E.P., Heinemann, M., 2018. Reassessing the role of the Escherichia coli CpxAR system in sensing surface contact. *PLoS One* **13**, 1–11. https://doi.org/10.1371/journal.pone.0207181

Kleinstreuer, N.C., Sullivan, K., Allen, D., Edwards, S., Mendrick, D.L., Embry, M., Matheson, J., Rowlands, J.C., Munn, S., Maull, E., Casey, W., 2016. Adverse outcome pathways: From research to regulation scientific workshop report. *Regul. Toxicol. Pharmacol.* **76**, 39–50. https://doi.org/10.1016/j.yrtph.2016.01.007

Li, N., Zeng, S., He, L., Zhong, W., 2010. Probing nanoparticle-protein interaction by capillary electrophoresis. *Anal. Chem.* **82**, 7460–7466. https://doi.org/10.1021/ac101627p

van Loosdrecht, M.C.M., Lyklema, J., Norde, W., Zehnder, A.J.B., 1990. Influence of interfaces on microbial activity. *Microbiol. Rev.* **54**, 75–87.

López-León, T., Carvalho, E.L.S., Seijo, B., Ortega-Vinuesa, J.L., Bastos-González, D., 2005. Physicochemical characterization of chitosan nanoparticles: Electrokinetic and stability behavior. *J. Colloid Interface Sci.* **283**, 344–351. https://doi.org/10.1016/j.jcis.2004.08.186

López-Viota, J., Mandal, S., Delgado, A. V., Toca-Herrera, J.L., Möller, M., Zanuttin, F., Balestrino, M., Krol, S., 2009. Electrophoretic characterization of gold nanoparticles functionalized with human serum albumin (HSA) and creatine. *J. Colloid Interface Sci.* **332**, 215–223. https://doi.org/10.1016/j.jcis.2008.11.077

Majdalani, N., Heck, M., Stout, V., Gottesman, S., 2005. Role of RcsF in signaling to the Rcs phosphorelay pathway in Escherichia coli. *J. Bacteriol.* **187**, 6770–6778. https://doi.org/10.1128/JB.187.19.6770-6778.2005

Malvern Instruments Limited, 2012. A basic guide to particle characterization. *White Pap.* 1–26. https://doi.org/10.1021/ac00110a016

Martinez-Gil, M., Goh, K.G.K., Rackaityte, E., Sakamoto, C., Audrain, B., Moriel, D.G., Totsika, M., Ghigo, J.M., Schembri, M.A., Beloin, C., 2017. YeeJ is an inverse autotransporter from Escherichia coli that binds to peptidoglycan and promotes biofilm formation. *Sci. Rep.* **7**, 1–16. https://doi.org/10.1038/s41598-017-10902-0

Mathelié-guinlet, M., 2017. Etude de l'intéraction nanoparticules-bactéries : application à l'élaboration d'un biocapteur. Université de Bordeaux.

Mathelié-Guinlet, M., Béven, L., Moroté, F., Moynet, D., Grauby-Heywang, C., Gammoudi, I., Delville, M.H., Cohen-Bouhacina, T., 2017. Probing the threshold of membrane damage and cytotoxicity effects induced by silica nanoparticles in Escherichia coli bacteria. *Adv. Colloid Interface Sci.* **245**, 81–91. https://doi.org/10.1016/j.cis.2017.04.012

Mathelié-Guinlet, M., Grauby-Heywang, C., Martin, A., Février, H., Moroté, F., Vilquin, A., Béven, L., Delville, M.H., Cohen-Bouhacina, T., 2018. Detrimental impact of silica nanoparticles on the nanomechanical properties of Escherichia coli, studied by AFM. *J. Colloid Interface Sci.* **529**, 53–

886 64. https://doi.org/10.1016/j.jcis.2018.05.098

887 Maurya, S.K., Gopmandal, P.P., Ohshima, H., 2018. Electrophoresis of concentrated suspension of
888 soft particles with volumetrically charged inner core. *Colloid Polym. Sci.* **296**, 721–732.
889 https://doi.org/10.1007/s00396-018-4292-0

890 McBroom, A.J., Kuehn, M.J., 2007. Release of outer membrane vesicles by Gram-negative bacteria is
891 a novel envelope stress response. *Mol. Microbiol.* **63**, 545–558. https://doi.org/10.1111/j.1365-
892 2958.2006.05522.x

893 Mecke, A., Majoros, I.J., Patri, A.K., Baker, J.R., Banaszak Holl, M.M., Orr, B.G., 2005. Lipid bilayer
894 disruption by polycationic polymers: The roles of size and chemical functional group. *Langmuir*
895 **21**, 10348–10354. https://doi.org/10.1021/la050629l

896 Monopoli, M.P., Åberg, C., Salvati, A., Dawson, K.A., 2012. Biomolecular coronas provide the
897 biological identity of nanosized materials. *Nat. Nanotechnol.* **7**, 779–786.
898 https://doi.org/10.1038/nnano.2012.207

899 Moore, M.N., 2006. Do nanoparticles present ecotoxicological risks for the health of the aquatic
900 environment? *Environ. Int.* **32**, 967–976. https://doi.org/10.1016/j.envint.2006.06.014

901 Moussa, M., Caillet, C., Town, R.M., Duval, J.F.L., 2015. Remarkable electrokinetic features of charge-
902 stratified soft nanoparticles: Mobility reversal in monovalent aqueous electrolyte. *Langmuir* **31**,
903 5656–5666. https://doi.org/10.1021/acs.langmuir.5b01241

904 Neal, A.L., 2008. What can be inferred from bacterium-nanoparticle interactions about the potential
905 consequences of environmental exposure to nanoparticles? *Ecotoxicology* **17**, 362–371.
906 https://doi.org/10.1007/s10646-008-0217-x

907 Ohshima, H., 1995. Electrophoresis of soft particles. *Adv. Colloid Interface Sci.* **62**, 189–235.
908 https://doi.org/10.1016/0001-8686(95)00279-Y

909 Pagnout, C., Jomini, S., Dadhwal, M., Caillet, C., Thomas, F., Bauda, P., 2012. Role of electrostatic
910 interactions in the toxicity of titanium dioxide nanoparticles toward Escherichia coli. *Colloids*
911 *Surfaces B Biointerfaces* **92**, 315–321. https://doi.org/10.1016/j.colsurfb.2011.12.012

912 Peulen, T.O., Wilkinson, K.J., 2011. Diffusion of nanoparticles in a biofilm. *Environ. Sci. Technol.* **45**,
913 3367–3373. https://doi.org/10.1021/es103450g

914 Phillips, R.L., Miranda, O.R., You, C.C., Rotello, V.M., Bunz, U.H.F., 2008. Rapid and efficient
915 identification of bacteria using gold-nanoparticle-poly(para-phenyleneethynylene) constructs.
916 *Angew. Chemie - Int. Ed.* **47**, 2590–2594. https://doi.org/10.1002/anie.200703369

917 Planchon, M., Ferrari, R., Guyot, F., Gélabert, A., Menguy, N., Chanéac, C., Thill, A., Benedetti, M.F.,
918 Spalla, O., 2013. Interaction between Escherichia coli and TiO2 nanoparticles in natural and
919 artificial waters. *Colloids Surfaces B Biointerfaces* **102**, 158–164.
920 https://doi.org/10.1016/j.colsurfb.2012.08.034

921 Reisner, A., Haagensen, J.A.J., Schembri, M.A., Zechner, E.L., Molin, S., 2003. Development and
922 maturation of Escherichia coli K-12 biofilms. *Mol. Microbiol.* **48**, 933–946. https://doi.org/3490
923 [pii]

924 Ribeiro, T., Baleizão, C., Farinha, J.P.S., 2017. Artefact-free evaluation of metal enhanced
925 fluorescence in silica coated gold nanoparticles. *Sci. Rep.* **7**, 1–12.
926 https://doi.org/10.1038/s41598-017-02678-0

927 Ribeiro, T., Raja, S., Rodrigues, A.S., Fernandes, F., Baleizão, C., Farinha, J.P.S., 2014. NIR and visible
928 perylenediimide-silica nanoparticles for laser scanning bioimaging. *Dye. Pigment.* **110**, 227–234.

https://doi.org/10.1016/j.dyepig.2014.03.026

Rowenczyk, L., Duclairoir-poc, C., Barreau, M., Picard, C., Hucher, N., Orange, N., Grisel, M., Feuilloley, M., 2017. Impact of coated TiO2-nanoparticles used in sunscreens on two representative strains of the human microbiota : Effect of the particle surface nature and aging. *Colloids Surfaces B Biointerfaces* **158**, 339–348. https://doi.org/10.1016/j.colsurfb.2017.07.013

Shang, L., Nienhaus, K., Nienhaus, G.U., 2014. Engineered nanoparticles interacting with cells: Size matters. *J. Nanobiotechnology* **12**, 1–11. https://doi.org/10.1186/1477-3155-12-5

Sheng, G.P., Yu, H.Q., Yue, Z.B., 2005. Production of extracellular polymeric substances from Rhodopseudomonas acidophila in the presence of toxic substances. *Appl. Microbiol. Biotechnol.* **69**, 216–222. https://doi.org/10.1007/s00253-005-1990-6

Shrivastava, S., Bera, T., Roy, A., 2007. Characterization of enhanced antibacterial effects of novel silver nanoparticles. *Nanotechnology* **18**. https://doi.org/10.1088/0957-4484/18/22/225103

Silva, T., Pokhrel, L.R., Dubey, B., Tolaymat, T.M., Maier, K.J., Liu, X., 2014. Particle size, surface charge and concentration dependent ecotoxicity of three organo-coated silver nanoparticles: Comparison between general linear model-predicted and observed toxicity. *Sci. Total Environ.* **468–469**, 968–976. https://doi.org/10.1016/j.scitotenv.2013.09.006

Silverman, P.M., 1997. Towards a structural biology of bacterial conjugation. *Mol. Microbiol.* **23**, 423–429. https://doi.org/10.1046/j.1365-2958.1997.2411604.x

Škvarla, J., 2007. Hard versus soft particle electrokinetics of silica colloids. *Langmuir* **23**, 5305–5314. https://doi.org/10.1021/la0635451

Stöber, W., Fink, A., Bohn, E., 1968. Controlled growth of monodisperse silica spheres in the micron size range. *J. Colloid Interface Sci.* **26**, 62–69. https://doi.org/10.1016/0021-9797(68)90272-5

Stoimenov, P.K., Klinger, R.L., Marchin, G.L., Klabunde, K.J., 2002. Metal oxide nanoparticles as bactericidal agents. *Langmuir* **18**, 6679–6686. https://doi.org/10.1021/la0202374

Svenson, S., 2009. Dendrimers as versatile platform in drug delivery applications. *Eur. J. Pharm. Biopharm.* **71**, 445–462. https://doi.org/10.1016/j.ejpb.2008.09.023

Tajarobi, F., El-Sayed, M., Rege, B.D., Polli, J.E., Ghandehari, H., 2001. Transport of poly amidoamine dendrimers across Madin-Darby canine kidney cells. *Int. J. Pharm.* **215**, 263–267. https://doi.org/10.1016/S0378-5173(00)00679-7

Thill, A., Zeyons, O., Spalla, O., Chauvat, F., Rose, J., Auffan, M., Flank, A.M., 2006. Cytotoxicity of CeO2 nanoparticles for Escherichia coli. Physico-chemical insight of the cytotoxicity mechanism. *Environ. Sci. Technol.* **40**, 6151–6156. https://doi.org/10.1021/es060999b

Velzeboer, I., Hendriks, A.J., Ragas, M.J., De Meent, D., 2008. Nanomaterials in the environment aquatic ecotoxicity tests of some nanomaterials. *Environ. Toxicol. Chem.* **27**, 1942–1947. https://doi.org/10.1897/07-509.1

Van Der Wal, A., Norde, W., Zehnder, A.J.B., Lyklema, J., 1997. Determination of the total charge in the cell walls of Gram-positive bacteria. *Colloids Surfaces B Biointerfaces* **9**, 81–100. https://doi.org/10.1016/S0927-7765(96)01340-9

Wang, Y.A., Yu, X., Silverman, P.M., Harris, R.L., Egelman, E.H., 2009. The structure of F-pili. *J. Mol. Biol.* **385**, 22–29. https://doi.org/10.1016/j.jmb.2008.10.054

Yang, Y., Quensen, J., Mathieu, J., Wang, Q., Wang, J., Li, M., Tiedje, J.M., Alvarez, P.J.J., 2013. Pyrosequencing reveals higher impact of silver nanoparticles than Ag+ on the microbial

971 community structure of activated sludge. *Water Res.* **48**, 317–325.
972 https://doi.org/10.1016/j.watres.2013.09.046

973 Zeyons, O., Thill, A., Chauvat, F., Menguy, N., Cassier-Chauvat, C., Oréar, C., Daraspe, J., Auffan, M.,
974 Rose, J., Spalla, O., 2009. Direct and indirect CeO2 nanoparticles toxicity for Escherichia coli and
975 Synechocystis. *Nanotoxicology* **3**, 284–295. https://doi.org/10.3109/17435390903305260

976

977

Tables

Table 1: Characteristics of the bacteria adopted in this work.

Strains	Expressed surface appendages	Genotype	Antibiotic resistance	Antibiotics for culture	Reference
E2152 (nude)	no flagella, no YeeJ protein, no Ag43, no type 1 fimbriae, no F factor	MG1655_gfp_Δfli _Δflu::km_ΔfimA-H::zeo	Amp^R, Cm^R, Km^R, Zeo^R	Ampicillin (Amp): 100 μg mL^{-1} Kanamycin (Km): 50 μg mL^{-1}	(Francius et al. 2011)
E2551 (YeeJ)	no flagella, no Ag43, no type 1 fimbriae, no F factor, constitutive expression of YeeJ	MG1655_gfp_Δfli _ Δflu_ΔfimA-H::zeo_kmPcLyeeJ	Amp^R, Cm^R, Km^R, Zeo^R	Ampicillin: 100 μg mL^{-1} Kanamycin: 50 μg mL^{-1}	(Martinez-Gil et al. 2017)
E2302 (F+)	no flagella, no Ag43, no type 1 fimbriae, no YeeJ protein, constitutive expression of F-pili	MG1655_gfp_Δfli_Δflu::km_ΔfimA-H::zeo_F'tet	Amp^R, Cm^R, Km^R, Zeo^R, Tet^R	Ampicillin: 100 μg mL^{-1} Tetracyclin (Tet): 50 μg mL^{-1}	(Francius et al. 2011)

Table 2: Values of charge density ρ_0 (in mM) and hydrodynamic penetration length $1/\lambda_0$ (in nm) obtained from **eqs 1-4** adopted to recover the electrokinetic data given in **Figure 1**. ρ_0 is expressed in molar concentration of equivalent monovalent cationic or anionic charges (depending on pH), *i.e.* the ratio between charge density (in C m^{-3}) and Faraday number.

$SiNH_2$ NPs	pH 3 and 4	pH 5	pH 6	pH 7	pH 9
ρ_0 (mM)	105	1.3	-17.7	-50.5	-73.7
$1/\lambda_0$ (nm)	0.74	1.07	1.00	1.11	1.30

Table 3: Values of charge density ρ_0 and hydrodynamic penetration length $1/\lambda_o$ at different pH values for the nude (E2152), YeeJ (E2551) and F-pili (E2302) strains obtained from Ohshima's model (**eqs 1-4**). ρ_0 is expressed in molar concentration of equivalent monovalent anionic charges, *i.e.* from the ratio between charge density (in C m^{-3}) and Faraday number.

	Nude (E2152)		YeeJ (E2551)		F-pili (E2302)	
	pH 3	pH 7	pH 3	pH 7	pH 3	pH 7
ρ_o (mM)	-57.5	-195	-53.7	-92.5	-64.6	-101

$1/\lambda_o$ (nm)	0.91	0.51	0.85	0.88	0.85	0.83

990

991 **Table 4: Values of the slopes ω corresponding to the linear plots σ_2 *vs.* σ_1** for nude (E2152), YeeJ
992 (E2551) and F-pili (E2302) cells at pH 7 and pH 3 in the absence or presence of $SiNH_2$ NPs (indicated).
993 Data correspond to mean values $\pm$ standard deviation as obtained from analysis of 3 to 7 cells per
994 examined condition. Data given at pH 3, without specification of standard deviation, correspond to
995 the analysis of 1 F-pili cell as we encountered significant difficulties in imaging more of these cells
996 under such pH condition, which is possibly due to AFM tip contamination by NPs and/or detached F-
997 pili structures during sample scanning (**Figure S2**).

	pH 7	$SiNH_2$ NPs pH 7	pH 3	$SiNH_2$ NPs pH 3
Nude (E2152)	0.64 ± 0.13	0.79 ± 0.07	0.61 ± 0.07	1.26 ± 0.50
YeeJ (E2551)	1.23 ± 0.17	1.01 ± 0.14	1.96 ± 0.30	1.29 ± 0.80
F-pili (E2302)	1.43 ± 0.15	0.85 ± 0.18	1.15	1.73

998